THE KRONECKER–WEYL EQUIDISTRIBUTION THEOREM AND GEODESICS IN 3-MANIFOLDS

J. BECK AND W.W.L. CHEN

ABSTRACT. Given any rectangular polyhedron 3-manifold $\mathcal{P}$ tiled with unit cubes, we find infinitely many explicit directions related to cubic algebraic numbers such that all half-infinite geodesics in these directions are uniformly distributed in $\mathcal{P}$.

1. INTRODUCTION

The long-term time evolution of linear flow in the flat torus has an established theory, which forms an important chapter in diophanine approximation. Here the *continuous* version of the classical Kronecker–Weyl equidistribution theorem can be formulated as follows; see [12].

Theorem A. *Let* $\mathbf{v} = (1, \gamma_1, \ldots, \gamma_m) \in \mathbb{R}^{m+1}$*, where* m *is a positive integer and the real numbers* $1, \gamma_1, \ldots, \gamma_m$ *are linearly independent over the rationals. Then any half-infinite geodesic with direction* $\mathbf{v}$ *is uniformly distributed in the unit torus* $[0,1]^{m+1}$*.*

Thus we have an essentially complete understanding of geodesics in the unit torus.

We use the two terms *uniformly distributed* and *equidistributed* with precisely the same meaning. Given any Jordan measurable test set $A \subseteq [0,1]^{m+1}$, the proportion of time the half-infinite geodesic with direction $\mathbf{v}$ falls into A is asymptotically equal to the $(m+1)$-dimensional volume of A.

Geodesic flow in the unit torus $[0,1]^{m+1}$ for positive integers m exhibits remarkable stability and predictability, justifying the intuitive term *integrable system*. Here two particles moving on two parallel geodesics close to each other with the same speed and direction remain close forever. However, this is not the case when we consider *non-integrable systems*. Figure 1.1 illustrates this point in the special case of the L-surface which clearly contains a singularity.

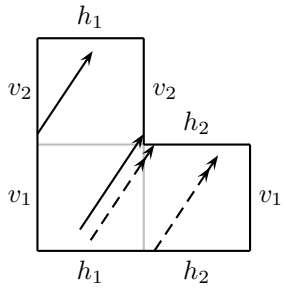

Figure 1.1: geodesic flow on the L-surface

One of the pioneering results concerning the equidistribution of geodesics on a large class of non-integrable flat surfaces is due to Gutkin [4] and Veech [11] in the 1980s, and represents the first extension of the 2-dimensional Kronecker–Weyl equidistribution theorem to non-integrable flat systems such as *polysquare surfaces*.

2010 *Mathematics Subject Classification.* 11K38, 37E35.

Key words and phrases. geodesics, billiards, equidistribution, density.

Before we proceed, let us define *polysquare region* and *polysquare surface*.

A *polysquare region* consists of a finite number of unit size squares such that (i) any two squares either are disjoint, or have a common edge, or have a common vertex; and (ii) there is edge-connectivity, that any two squares are joined by a chain of squares such that any two consecutive members of the chain share a common edge. Note that a polysquare region has boundary.

To obtain a polysquare surface, or square tiled surface, we divide the collection of the horizontal boundary edges of the polysquare region into identified pairs, and divide the collection of the vertical boundary edges of the polysquare region into identified pairs. In this way, we obtain a closed surface equipped with a flat metric, so that it is a Riemann surface, with possible canonical singularities, where every square has zero curvature. We then refer to such a polysquare surface as a *translation surface*. Geodesic flow on a flat translation surface is 1-direction linear flow.

The following result is often known as the Gutkin–Veech theorem.

Theorem B. *A geodesic on any polysquare surface, with any starting point and any irrational slope, is equidistributed, unless it hits a singular point and becomes undefined.*

Given the gap of about 70 years between the Kronecker–Weyl equidistribution theorem and the Gutkin–Veech theorem, it is quite clear that the singularities in non-integrable systems lead to considerable difficulties. On the other hand, a very natural question that arises from the Gutkin–Veech theorem concerns possible extensions of the Kronecker–Weyl equidistribution theorem to non-integrable systems along similar lines but in higher dimensions. Observe that the Gutkin–Veech theorem is about 2-dimensional non-integrable flat systems. The methods there, unfortunately, do not seem to extend to the case of flat systems in higher dimensions. Indeed, as far as we are aware, there is no uniformity result in the literature concerning geodesics in 3-manifolds along these lines. The object of this paper is to study uniformity of half-infinite 1-direction geodesics in *polycube* 3*-manifolds* and related questions.

Before we proceed, let us define *polycube region* and *polycube* 3*-manifold*.

A *polycube region* consists of a finite number of unit size cubes such that (i) any two cubes either are disjoint, or have a common face, or have a common edge, or have a common vertex; and (ii) there is face-connectivity, that any two cubes are joined by a chain of cubes such that any two consecutive members of the chain share a common face. Note that a polycube region has boundary.

To obtain a polycube 3-manifold, or cube tiled manifold, we divide the collection of the xy-parallel faces of the polycube region into identified pairs, divide the collection of the xz-parallel faces of the polycube region into identified pairs, and divide the collection of the yz-parallel faces of the polycube region into identified pairs. In this way, we obtain a closed 3-manifold equipped with a flat metric, with possible canonical singularities. We then refer to such a polycube 3-manifold as a *translation* 3*-manifold*. Geodesic flow on a flat translation 3-manifold is 1-direction linear flow.

The known techniques seem to fall well short for establishing any comparable analog of the Gutkin–Veech theorem in this 3-dimensional setting. Nevertheless, we can prove that for any given polycube 3-manifold $\mathcal{P}$, there are infinitely many special directions, which can be given explicitly, such that every half-infinite geodesic having such a direction is uniformly distributed in $\mathcal{P}$.

A street in a polycube 3-manifold $\mathcal{P}$ denotes a *maximal* cycle of consecutive unit cubes arranged in a linear fashion along one of the 3 coordinate directions, forming a *cyclic solid cylinder*. Thus there are X-streets, Y-streets and Z-streets, where, for

instance, a Z-street denotes a box of the form

$$[a, a+1] \times [b, b+1] \times [c, c+\ell], \quad a, b, c, \ell \in \mathbb{Z},$$

where the side of length $\ell \geqslant 1$ is parallel to the Z-axis. It is natural to call the integer ℓ the length of the street. The *street-LCM* of $\mathcal{P}$ is the least common multiple of the lengths of the streets of $\mathcal{P}$.

Using a new method, we can prove the following result.

Theorem 1. *Let $\mathcal{P}$ be an arbitrary polycube 3-manifold, and let $h = h(\mathcal{P})$ denote the street-LCM of $\mathcal{P}$.*

(i) *Let $k \geqslant 1$ be any fixed integer, and let α_k be the root of the cubic equation*

$$x^3 + hkx - 1 = 0, \quad \frac{1}{hk+1} < x < \frac{1}{hk}. \tag{1.1}$$

Write

$$\mathbf{v}_0 = (\alpha_k, \alpha_k^2, 1), \quad \mathbf{v}_1 = (1, \alpha_k, \alpha_k^2), \quad \mathbf{v}_2 = (\alpha_k^2, 1, \alpha_k). \tag{1.2}$$

Then every half-infinite geodesic with direction given by $\mathbf{v}_i$, $i = 0, 1, 2$, exhibits uniformity in $\mathcal{P}$, provided that the integer parameter k is sufficiently large depending only on $\mathcal{P}$. The test sets for uniformity are all 3-dimensional Jordan measurable subsets of $\mathcal{P}$.

(ii) *Let A be an arbitrary 3-dimensional Jordan measurable set in $\mathcal{P}$, and let $L(t)$, $0 \leqslant t \leqslant T$, be a finite geodesic with direction given by $\mathbf{v}_i$, $i = 0, 1, 2$, in (1.1)–(1.2), with arc-length parametrization. Then there exist effectively computable explicit positive constants $c_1 = c_1(A; \alpha_k) > 0$ and $c_2 = c_2(A; \alpha_k) > 0$ such that*

$$|\{0 \leqslant t \leqslant T : L(t) \in A\}| \geqslant c_1 T,$$

provided that $T \geqslant c_2$.

Part (i) is a time-qualitative result that does not say anything about the speed of convergence to uniformity. However, it is complemented by part (ii), which is a time-quantitative result exhibiting at least a weaker form of uniformity.

Theorem 1 only gives a small collection of slopes. The majority of the remaining directions remain currently out of reach. We also do not know what happens beyond the class of polycube 3-manifolds.

We mention here that Theorems A, B and 1 have analogs on billiard in the unit cube, a polysquare region and a polycube region respectively, via a simple but very important discovery made more than 100 years ago by König and Szücs [6]. The underlying geometric trick is called *unfolding*. We illustrate the idea in the case of the unit square $[0, 1]^2$ in Figure 1.2, where the 2×2 torus in the picture on the right is a 4-fold covering of the unit square. Billiard flow in the square on the left is equivalent to geodesic flow in the torus on the right.

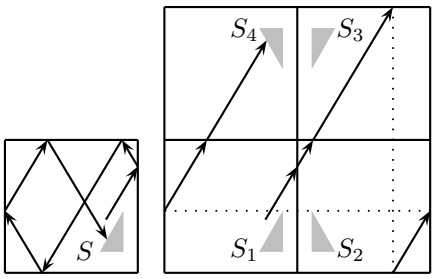

Figure 1.2: unfolding a billiard orbit in the unit torus $[0, 1]^2$

For further reading on the ergodic theory of flat surfaces, the reader is referred to the survey papers [5, 8, 9, 13].

2. Geodesics in the L-solid manifold

We begin the proof of Theorem 1 with a discussion of the special case when the polycube 3-manifold in question is obtained as a translation 3-manifold from the L-solid region shown in Figure 2.1. Here the 3 unit cubes of the region are called the *top cube*, the *middle cube* and the *right cube*. The street-LCM of the resulting L-solid 3-manifold is 2. We shall consider geodesics inside this manifold and, in particular, those with directions given by (1.1)–(1.2).

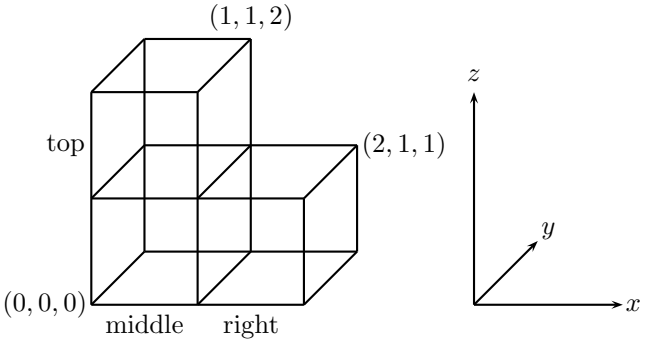

Figure 2.1: the L-solid region

For convenience, we refer to the L-solid region or the L-solid 3-manifold simply as the L-solid.

We introduce a convenient labelling of the faces of the L-solid; see Figures 2.1–2.3.

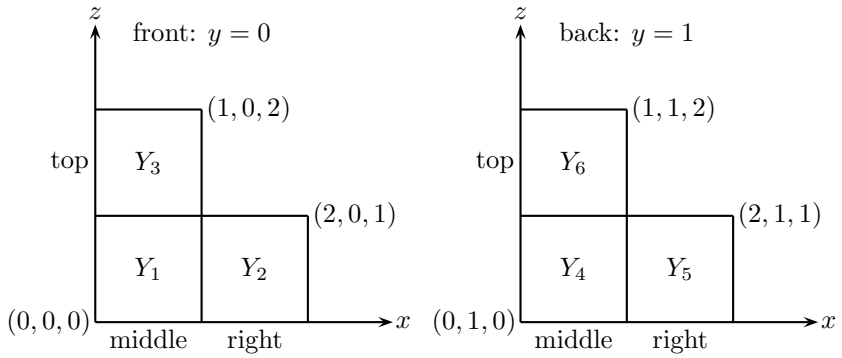

Figure 2.2: labelling the front and back faces of the L-solid

The picture on the left in Figure 2.2 shows the 3 front faces of the L-solid, with $y = 0$. The front top square face Y_3 has vertices $(0, 0, 1), (1, 0, 1), (0, 0, 2), (1, 0, 2)$. We denote this fact by

$$Y_3 = \mathrm{SQ}\{(0, 0, 1), (1, 0, 1), (0, 0, 2), (1, 0, 2)\}.$$

The front middle and front right square faces are denoted respectively by

$$Y_1 = \mathrm{SQ}\{(0, 0, 0), (1, 0, 0), (0, 0, 1), (1, 0, 1)\},$$
$$Y_2 = \mathrm{SQ}\{(1, 0, 0), (2, 0, 0), (1, 0, 1), (2, 0, 1)\}.$$

On the other hand, the picture on the right in Figure 2.2 shows the 3 back faces of the L-solid, with $y = 1$. The back top, back middle and back right square faces are denoted respectively by

$$Y_6 = \mathrm{SQ}\{(0, 1, 1), (1, 1, 1), (0, 1, 2), (1, 1, 2)\},$$
$$Y_4 = \mathrm{SQ}\{(0, 1, 0), (1, 1, 0), (0, 1, 1), (1, 1, 1)\},$$
$$Y_5 = \mathrm{SQ}\{(1, 1, 0), (2, 1, 0), (1, 1, 1), (2, 1, 1)\}.$$

These 6 square faces are perpendicular to the y-axis, justifying use of the letter Y.

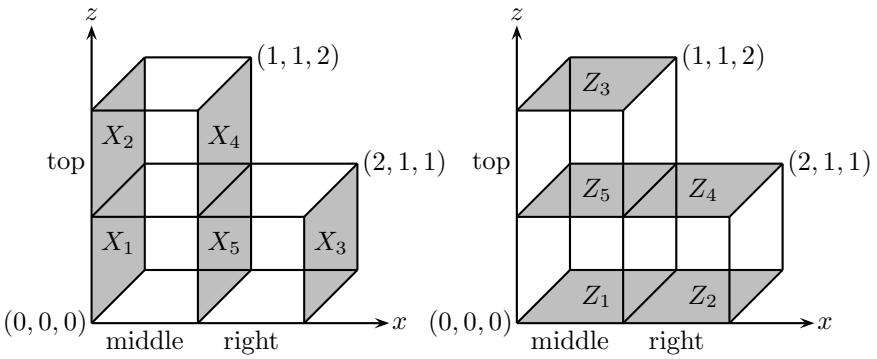

Figure 2.3: labelling the rest of the faces of the L-solid

We see from Figure 2.3 that between the front and back faces, there are 4 faces

$$X_1 = \mathrm{SQ}\{(0,0,0),(0,1,0),(0,0,1),(0,1,1)\},$$
$$X_2 = \mathrm{SQ}\{(0,0,1),(0,1,1),(0,0,2),(0,1,2)\},$$
$$X_3 = \mathrm{SQ}\{(2,0,0),(2,1,0),(2,0,1),(2,1,1)\},$$
$$X_4 = \mathrm{SQ}\{(1,0,1),(1,1,1),(1,0,2),(1,1,2)\},$$

on the boundary of the L-solid that are perpendicular to the x-axis, another 4 faces

$$Z_1 = \mathrm{SQ}\{(0,0,0),(1,0,0),(0,1,0),(1,1,0)\},$$
$$Z_2 = \mathrm{SQ}\{(1,0,0),(2,0,0),(1,1,0),(2,1,0)\},$$
$$Z_3 = \mathrm{SQ}\{(0,0,2),(1,0,2),(0,1,2),(1,1,2)\},$$
$$Z_4 = \mathrm{SQ}\{(1,0,1),(2,0,1),(1,1,1),(2,1,1)\},$$

on the boundary of the L-solid that are perpendicular to the z-axis, and two inside faces

$$X_5 = \mathrm{SQ}\{(1,0,0),(1,1,0),(1,0,1),(1,1,1)\},$$
$$Z_5 = \mathrm{SQ}\{(0,0,1),(1,0,1),(0,1,1),(1,1,1)\}.$$

Let $k \geqslant 1$ be an arbitrary but fixed integer. Assume that a segment of a geodesic $\mathcal{L}_k$ starts from the origin $\mathbf{0} = (0,0,0)$ and ends at a point $C = (1,x,y)$ on the inside square face X_5, and in between hits the square face Z_3 on k separate occasions; see Figure 2.4, which shows the special case $k = 1$.

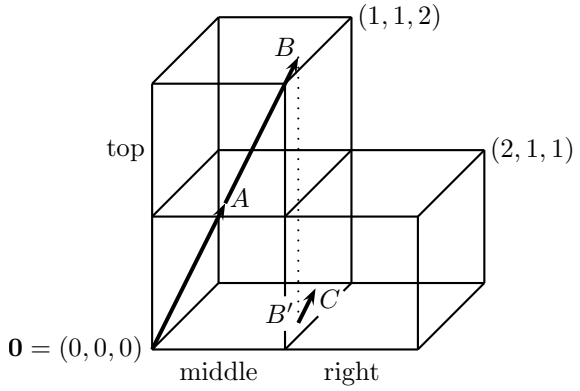

Figure 2.4: first detour crossing in the L-solid: the case $k = 1$

Let B denote the point on the square face Z_3 that $\mathcal{L}_k$ hits on the last occasion before it bounces down to the point B' and continues towards the point C.

Let A denote the point on the inside square face Z_5 that $\mathcal{L}_k$ hits on the first occasion, and assume that $A = (x, y, 1)$, so that its coordinates form a permutation of the coordinates of $C = (1, x, y)$ with the same quantities x and y. It is easy to see that $B = (2kx, 2ky, 2)$ and $B' = (2kx, 2ky, 0)$. The geometric fact that the two vectors $\mathbf{0}A$ and $B'C$ are parallel gives rise to the equations

$$\frac{1-2kx}{x} = \frac{x-2ky}{y} = \frac{y-0}{1}.$$

The first equality reduces to $y = x^2$. Substituting this into the right hand side and then equating with the left hand side, we conclude that

$$y = x^2 \quad \text{and} \quad x^3 + 2kx - 1 = 0. \tag{2.1}$$

Note that the cubic polynomial $x^3 + 2kx - 1$ is strictly increasing and has precisely one root α_k satisfying

$$\frac{1}{2k+1} < \alpha_k < \frac{1}{2k}. \tag{2.2}$$

Of course, (2.1)–(2.2) represent the special case of (1.1) when $h = 2$, the street-LCM of the L-solid.

We now take $x = \alpha_k$ and $y = \alpha_k^2$, and consider the segment of the geodesic $\mathcal{L}_k$ with direction vector $\mathbf{v}_0 = (\alpha_k, \alpha_k^2, 1)$ illustrated in Figure 2.4. Starting from the origin $\mathbf{0} = (0, 0, 0)$, this geodesic segment exhibits up-and-down zigzagging, and finally ends its journey at the point $C = (1, \alpha_k, \alpha_k^2)$ on the middle square face X_5. It represents a *left to right detour crossing* inside a tower-like 3-dimensional *street*, where the latter is the union of the middle cube and the top cube. Observe that with $0 < \alpha_k < 1$, the geodesic $\mathcal{L}_k$ goes to the right faster than it goes to the back, and so crosses from one X-face to another faster than crossing from one Y-face to another.

The straight line segment joining the two endpoints $\mathbf{0}$ and $C = (1, \alpha_k, \alpha_k^2)$ of this detour crossing is called the *shortcut* of this detour crossing.

The first extension of this particular zigzagging segment of the geodesic $\mathcal{L}_k$ with direction vector $\mathbf{v}_0 = (\alpha_k, \alpha_k^2, 1)$ starts from the point $C = (1, \alpha_k, \alpha_k^2)$ on the square face X_5 and goes to the point $D = (2, 2\alpha_k, 2\alpha_k^2)$ on the right face X_3; see Figure 2.5. This zigzagging extension hits the square face Z_4 on $2k$ separate occasions, at the points $(1 + i\alpha_k - \alpha_k^3, \alpha_k + i\alpha_k^2 - \alpha_k^4, 1)$, $1 \leqslant i \leqslant 2k$, before ending at the point D on the square face X_3.

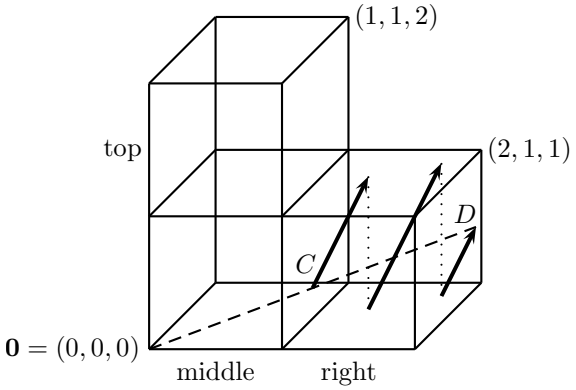

Figure 2.5: second detour crossing in the L-solid: the case $k = 1$

This zigzagging second segment of the geodesic $\mathcal{L}_k$ from C to D with direction vector $\mathbf{v}_0$ represents a *left to right detour crossing* inside a 3-dimensional *street*, which is simply the right cube. Again the straight line segment joining the two

endpoints C and D of this detour crossing is called the *shortcut* of this detour crossing.

These two shortcuts $\mathbf{0}C$ and CD, with endpoints $\mathbf{0} = (0, 0, 0)$, $C = (1, \alpha_k, \alpha_k^2)$ and $D = (2, 2\alpha_k, 2\alpha_k^2)$, are clearly collinear. In fact, the point C is the midpoint of the line segment $\mathbf{0}D$.

It is easy to see that this collinearity of the shortcuts is preserved as we continue and take the third, fourth and subsequent segments of the geodesic $\mathcal{L}_k$ starting from the origin with direction vector $\mathbf{v}_0 = (\alpha_k, \alpha_k^2, 1)$. This collinearity means precisely that these consecutive shortcuts together form another geodesic $\mathcal{L}_k^*$ starting from the origin, but it has a new direction vector $\mathbf{v}_1 = (1, \alpha_k, \alpha_k^2)$ obtained by a permutation of the coordinates of $\mathbf{v}_0$. We refer to this new geodesic $\mathcal{L}_k^*$ as the *shortline* of the original geodesic $\mathcal{L}_k$. Formally, $\mathbf{S}(\mathcal{L}_k) = \mathcal{L}_k^*$, where $\mathbf{S}$ denotes the *shortline operation*. In the special case $k = 1$, Figure 2.6 is basically Figures 2.4–2.5 put together. It shows the two parts of the zigzagging $\mathcal{L}_k$ from $\mathbf{0}$ to D, with the point C separating the two parts. It also shows the corresponding shortline segment of $\mathcal{L}_k^*$, indicated by the dashed arrow, from $\mathbf{0}$ to D.

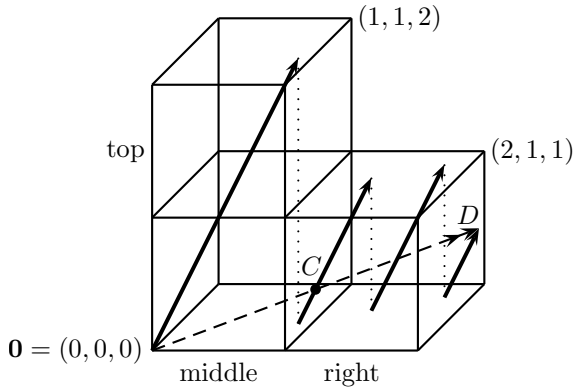

Figure 2.6: detour crossing and its shortline in the L-solid: the case $k = 1$

The crucial fact is that the geodesic $\mathcal{L}_k$ and its shortline $\mathcal{L}_k^*$ hit every square face X_i, $1 \leqslant i \leqslant 5$, at precisely the same points, like C and D in Figures 2.5–2.6. We refer to this observation as the *X-face hitting property* of the infinite geodesic $\mathcal{L}_k$ and its shortline $\mathcal{L}_k^*$.

The direction vector $\mathbf{v}_1 = (1, \alpha_k, \alpha_k^2)$ is clearly obtained from the direction vector $\mathbf{v}_0 = (\alpha_k, \alpha_k^2, 1)$ by a left shift in the cyclic permutation of the coordinates

$$1 \to \alpha_k \to \alpha_k^2 \to 1.$$

Applying a second left shift in this cyclic permutation, we obtain in turn a new direction vector $\mathbf{v}_2 = (\alpha_k^2, 1, \alpha_k)$. It is easy to see that the shortline of the geodesic $\mathcal{L}_k^*$ is a new geodesic $\mathcal{L}_k^{**}$ that starts at the origin and has direction vector $\mathbf{v}_2$. Formally, $\mathbf{S}(\mathcal{L}_k^*) = \mathcal{L}_k^{**}$. Note that $\mathcal{L}_k^*$ consists of *front to back detour crossings*, and $\mathcal{L}_k^{**}$ is the union of the corresponding shortcuts. Observe that with $0 < \alpha_k < 1$, the geodesic $\mathcal{L}_k^*$ goes to the back faster than it goes up, and so crosses from one Y-face to another faster than crossing from one Z-face to another.

Again the crucial fact is that the geodesic $\mathcal{L}_k^*$ and its shortline $\mathcal{L}_k^{**}$ hit every square face Y_i, $1 \leqslant i \leqslant 6$, at precisely the same points. We refer to this observation as the *Y-face hitting property* of the infinite geodesic $\mathcal{L}_k^*$ and its shortline $\mathcal{L}_k^{**}$.

Applying a third left shift in the cyclic permutation, we return to the original direction vector $\mathbf{v}_0 = (\alpha_k, \alpha_k^2, 1)$. It is easy to see that the shortline of the geodesic $\mathcal{L}_k^{**}$ is the original geodesic $\mathcal{L}_k$ that starts at the origin and has direction vector $\mathbf{v}_0$.

Formally, $\mathbf{S}(\mathcal{L}_k^{**}) = \mathcal{L}_k$. Note that $\mathcal{L}_k^{**}$ consists of *bottom to top detour crossings*, and $\mathcal{L}_k$ is the union of the corresponding shortcuts. Observe that with $0 < \alpha_k < 1$, the geodesic $\mathcal{L}_k^{**}$ goes up faster than it goes to the right, and so crosses from one Z-face to another faster than crossing from one X-face to another.

Again the crucial fact is that the geodesic $\mathcal{L}_k^{**}$ and its shortline $\mathcal{L}_k$ hit every square face Z_i, $1 \leqslant i \leqslant 5$, at precisely the same points. We refer to this observation as the *Z-face hitting property* of the infinite geodesic $\mathcal{L}_k^{**}$ and its shortline $\mathcal{L}_k$.

The remarkable face hitting properties explain why we focus on geodesics with direction given by one of the vectors

$$\mathbf{v}_0 = (\alpha_k, \alpha_k^2, 1), \quad \mathbf{v}_1 = (1, \alpha_k, \alpha_k^2), \quad \mathbf{v}_2 = (\alpha_k^2, 1, \alpha_k). \tag{2.3}$$

We shall prove uniformity of such geodesics in the L-solid by applying an adaptation of an *area magnification process via shortlines*, developed in [1, Section 6.3]. To make the present paper self-contained, we shall explain this magnification process in full details in Sections 3 and 4.

In [1, Section 6.3], we can establish *time-quantitative density*. In fact, we can establish a nearly optimal form of density of such geodesics in the L-solid. To explain this, let $\eta > 0$ be an arbitrarily small but fixed positive number. We say that a half-infinite geodesic $\mathcal{L}$ in the L-solid is *η-nearly superdense* if there exists an effectively computable explicit threshold $N_0(\eta)$ such that, for every integer $n \geqslant N_0(\eta)$, the initial segment of $\mathcal{L}$ with length $n^{2+\eta}$ intersects every axis-parallel cube of side length $1/n$ in the L-solid.

Remark. The optimal property would be to replace $n^{2+\eta}$ by a constant multiple of n^2. We call this superdensity. Unfortunately we are not able to establish superdensity in the 3-dimensional case.

The following result is [1, Theorem 6.1.2].

Time-quantitative Density A. *Let $\eta > 0$ be fixed. There exists a threshold $K_0(\eta)$ such that for every integer $k \geqslant K_0(\eta)$, any half-infinite geodesic in the L-solid with direction given by one of the vectors in* (2.3)*, where α_k is a root of the cubic equation $x^3 + 2kx - 1 = 0$ satisfying* (2.2)*, is η-nearly superdense in the L-solid.*

In fact, we need only a straightforward corollary of the above result, obtained by choosing *any* fixed value of η in the interval $0 < \eta < 1$.

Time-quantitative Density B. *Let $k \geqslant K_0$, where K_0 is an effectively computable sufficiently large absolute constant. Let $\kappa > 0$ be arbitrarily small but fixed. Then there exists an explicit threshold $C^\star = C^\star(\kappa; k)$ such that every geodesic segment in the L-solid with length $C^\star$ and direction given by one of the vectors in* (2.3)*, where α_k is a root of the cubic equation $x^3 + 2kx - 1 = 0$ satisfying* (2.2)*, intersects every square of side length κ on the surface of the L-solid.*

Our first goal is to establish uniformity of these special geodesics in the L-solid. Unfortunately, our proof does not give any error term, so what we can prove here is time-qualitative uniformity. The proof consists of four major steps:

(i) preparation for the magnification process;
(ii) the magnification process;
(iii) grids and iteration; and
(iv) conclusion via the Time-quantitative Density B.

We shall cover these in the next four sections.

3. Preparation for the magnification process

We shall use Birkhoff's well known pointwise ergodic theorem concerning measure preserving systems $(X, \mathcal{A}, \mu, T)$. The triple $(X, \mathcal{A}, \mu)$ is a measure space, where X is the underlying space, $\mathcal{A}$ is a σ-algebra of sets in X, while μ is a non-negative σ-additive measure on X with $\mu(X) < \infty$, and $T : X \to X$ is a measure-preserving transformation, so that $T^{-1}A \in \mathcal{A}$ and $\mu(T^{-1}A) = \mu(A)$ for every $A \in \mathcal{A}$. Here we simply apply ergodic theory, and do not expect the reader to have any serious expertise in the subject. Knowledge of Lebesgue integral and basic measure theory suffices.

Let $L^1(X, \mathcal{A}, \mu)$ denote the space of measurable and integrable functions in the measure space $(X, \mathcal{A}, \mu)$. Then Birkhoff's pointwise ergodic theorem says that for every function $f \in L^1(X, \mathcal{A}, \mu)$, the limit

$$\lim_{m\to\infty} \frac{1}{m} \sum_{j=0}^{m-1} f(T^j x) = f^*(x) \tag{3.1}$$

exists for μ-almost every $x \in X$, where $f^* \in L^1(X, \mathcal{A}, \mu)$ is a T-invariant measurable function satisfying the condition

$$\int_X f \,\mathrm{d}\mu = \int_X f^* \,\mathrm{d}\mu.$$

A particularly important special case is when T is *ergodic*, when every measurable T-invariant set $A \in \mathcal{A}$ is *trivial* in the precise sense that $\mu(A) = 0$ or $\mu(A) = \mu(X)$. This is equivalent to the assertion that every measurable T-invariant function is constant μ-almost everywhere.

If T is ergodic, then (3.1) simplifies to

$$\lim_{m\to\infty} \frac{1}{m} \sum_{j=0}^{m-1} f(T^j x) = \int_X f \,\mathrm{d}\mu, \tag{3.2}$$

and the right-hand side of (3.1) is the same constant for μ-almost every $x \in X$.

The remarkable intuitive interpretation of (3.2) is that the *time average* on the left hand side is equal to the *space average* on the right hand side.

Unfortunately, Birkhoff's theorem does not give the speed of convergence in (3.1) or (3.2).

Next we explain how ergodicity and Birkhoff's theorem is used in the proof. Recall the labelling of the square faces of the L-solid shown in Figures 2.2–2.3. Consider the 5 square faces X_i, $1 \leqslant i \leqslant 5$, each with area 1. Boundary identification in the L-solid gives $X_1 = X_3$ and $X_2 = X_4$, so that we simply have the 3 square faces X_1, X_2, X_5. We define our underlying measure space as the set $X_0 = X_1 \cup X_2 \cup X_5$ with the usual area, or 2-dimensional Lebesgue measure, denoted by $\lambda(\cdot)$. Then X_0 is in fact a compact flat surface, *i.e.*, polysquare surface, of area 3, so that $\lambda(X_0) = 3$.

We shall use the special direction $\mathbf{v}_1 = (1, \alpha_k, \alpha_k^2)$, where α_k is a root of the cubic equation $x^3 + 2kx - 1 = 0$ satisfying (2.2).

The $\mathbf{v}_1$-flow in the L-solid defines a λ-preserving transformation on X_0 in the natural way as illustrated in Figure 3.1. For instance, the point $C \in X_5$ is mapped to the point $D \in X_3 = X_1$ via the $\mathbf{v}_1$-flow. Similarly, the $\mathbf{v}_1$-flow maps almost every point of the *measure-space* X_0 to another point of X_0; here we ignore the singularities. Let $T = T_{\mathbf{v}_1} : X_0 \to X_0$ denote this λ-preserving transformation. In particular, $T(C) = D$ in Figure 3.1.

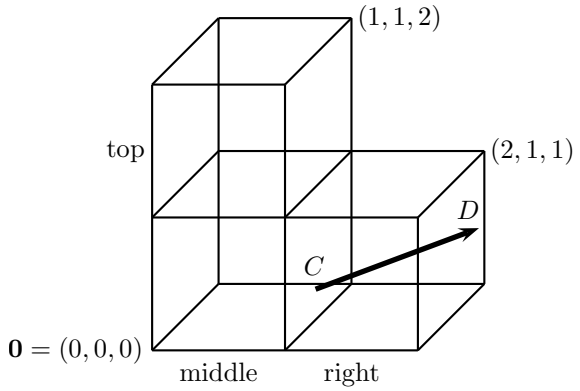

Figure 3.1: transformation $T = T_{\mathbf{v}_1}$, where $\mathbf{v}_1 = CD$

The major part of our argument is to prove that this particular transformation $T = T_{\mathbf{v}_1}$ is ergodic. In other words, we need to show that if $S \subset X_0$ is a measurable T-invariant set, then $\lambda(S) = 0$ or $\lambda(S) = 3$. Once ergodicity is established, it is relatively straightforward to derive uniformity via Birkhoff's theorem, at least for almost every starting point.

We shall prove ergodicity by contradiction. Assume on the contrary that there is a *non-trivial* measurable T-invariant set $S_0 \subset X_0$ such that $0 < \lambda(S_0) < 3$. We shall then derive a contradiction by using a version of the magnification process via shortlines developed in [1, Sections 6.2–6.3]. Note that our assumption ensures that the complement $S_0^c = X_0 \setminus S_0$ is another non-trivial measurable T-invariant set.

Removing a set of measure zero, we can clearly assume that for every point $x \in S_0$, $T^j x$ is well defined for every $j \geqslant 1$.

Given a point $z \in X_0$ and a radius $0 < r < 1/2$, let $D(z; r)$ denote the circular disk of radius r and centered at z. Then $D(z; r)$ has area $r^2\pi$. Note that $D(z; r) \subset X_0$, due to the fact that X_0 is a compact flat surface. Lebesgue's density theorem then says that, for almost every $z \in S_0$,

$$\lim_{r \to 0} \frac{\lambda(S_0 \cap D(z; r))}{r^2\pi} = 1,$$

and for almost every $z \in S_0^c = X_0 \setminus S_0$,

$$\lim_{r \to 0} \frac{\lambda(S_0 \cap D(z; r))}{r^2\pi} = 0.$$

Let $n \geqslant 1$ be an integer, and divide each of the square faces X_1, X_2, X_5 into n^2 congruent squares of area n^{-2} in the standard way. We shall refer to them as *small n-squares*. Thus we have $3n^2$ small n-squares in X_0.

Lemma 3.1. *Suppose that the real number τ satisfies*

$$3 > \tau = \lambda(S_0^c) > 0 \quad \textit{and} \quad 3 > 3 - \tau = \lambda(S_0) > 0. \tag{3.3}$$

Let $\varepsilon > 0$ be arbitrarily small but fixed. Then there exists a finite integer-valued threshold $n = n(S_0; \varepsilon)$ such that there exist at least $(\tau - \varepsilon)n^2$ small n-squares Q with

$$\frac{\lambda(S_0 \cap Q)}{(1/n)^2} < \varepsilon. \tag{3.4}$$

Proof. Since $S_0^c = X_0 \setminus S_0$ is Lebesgue measurable, given any $\delta > 0$, there exist finitely many disjoint axis-parallel rectangles such that their union V is δ-close to $S_0^c = X_0 \setminus S_0$ in the sense of the measure of the symmetric difference, so that

$$\lambda(V \setminus S_0^c) + \lambda(S_0^c \setminus V) < \delta.$$

It follows that

$$\lambda(V) > \lambda(S_0^c) - \delta = \tau - \delta \quad \text{and} \quad \lambda(S_0 \cap V) < \delta.$$

Since V is a finite union of disjoint axis-parallel rectangles, there clearly exists an integer-valued threshold $n = n(V;\delta)$ such that the union V_1 of the small n-squares Q contained in V has measure at least

$$\lambda(V_1) > \lambda(V) - \delta > \tau - 2\delta.$$

Let $\mathcal{B}$ denote the set of n-squares Q that do not satisfy (3.4), so that

$$\frac{\lambda(S_0 \cap Q)}{(1/n)^2} \geqslant \varepsilon.$$

Then

$$\delta > \lambda(S_0 \cap V) \geqslant \lambda(S_0 \cap V_1) = \sum_{Q \subseteq V_1} \lambda(S_0 \cap Q) \ \geqslant \sum_{Q \in \mathcal{B}} \lambda(S_0 \cap Q) \geqslant \frac{\varepsilon |\mathcal{B}|}{n^2},$$

so that

$$|\mathcal{B}| \leqslant \frac{\delta n^2}{\varepsilon} = \frac{\varepsilon n^2}{3},$$

if we take $\delta = \varepsilon^2/3$. We may assume without loss of generality that $0 < \varepsilon < 1$. Deleting the n-squares $Q \in \mathcal{B}$, we see that V_1 contains at least

$$(\tau - 2\delta)n^2 - \frac{\varepsilon n^2}{3} = \left(\tau - \frac{2\varepsilon^2}{3} - \frac{\varepsilon}{3}\right) n^2 > (\tau - \varepsilon)n^2$$

n-squares Q that satisfy (3.4). Finally, note that V and δ depend on S_0 and ε. □

We now continue our discussion under the assumptions of Lemma 3.1.

Let $\mathcal{Q}$ denote the set of small n-squares Q that satisfy the bound (3.4). For notational convenience, we may write

$$\mathcal{Q} = \{Q_i : i \in I\}. \tag{3.5}$$

Then, in view of Lemma 3.1, we have

$$|I| = |\mathcal{Q}| \geqslant (\tau - \varepsilon)n^2. \tag{3.6}$$

For every $i \in I$ in (3.5), let χ_i denote the characteristic function of the subset $S_0 \cap Q_i$ of X_0, so that

$$\chi_i(x) = \begin{cases} 1, & \text{if } x \in S_0 \cap Q_i, \\ 0, & \text{otherwise.} \end{cases}$$

Applying Birkhoff's theorem in the form (3.1) to each function χ_i, $i \in I$, we have

$$\lim_{m \to \infty} \frac{1}{m} \sum_{j=0}^{m-1} \chi_i(T^j x) = \chi_i^*(x), \tag{3.7}$$

for μ-almost every $x \in X_0$, where each $\chi_i^*(x)$ is some T-invariant measurable function satisfying the condition

$$\int_{X_0} \chi_i^*(x)\,\mathrm{d}x = \int_{X_0} \chi_i(x)\,\mathrm{d}x = \lambda(S_0 \cap Q_i). \tag{3.8}$$

Combining (3.4) and (3.8), for every $i \in I$, we have

$$\int_{X_0} \left(\frac{1}{|I|} \sum_{i \in I} \chi_i^*(x) \right) \mathrm{d}x = \frac{1}{|I|} \sum_{i \in I} \lambda(S_0 \cap Q_i) < \frac{\varepsilon}{n^2}. \tag{3.9}$$

Using the left-hand side of (3.7), we deduce that $\chi_i^*(x)$ is non-negative μ-almost everywhere. It then follows from (3.9) that

$$\frac{1}{\lambda(S_0)}\int_{S_0}\left(\frac{1}{|I|}\sum_{i\in I}\chi_i^*(x)\right)\mathrm{d}x \leqslant \frac{1}{\lambda(S_0)}\int_{X_0}\left(\frac{1}{|I|}\sum_{i\in I}\chi_i^*(x)\right)\mathrm{d}x < \frac{1}{\lambda(S_0)}\frac{\varepsilon}{n^2}. \quad (3.10)$$

Taking the minimum of the function

$$g(x) = \frac{1}{|I|}\sum_{i\in I}\chi_i^*(x)$$

over $x \in S_0$, or getting arbitrarily close to that, (3.10) implies the existence of some $x_0 \in S_0$ such that

$$0 \leqslant \frac{1}{|I|}\sum_{i\in I}\chi_i^*(x_0) < \frac{\varepsilon}{(3-\tau)n^2}, \quad (3.11)$$

where the factor $3-\tau$ in the denominator at the right hand side is the measure of S_0 given by (3.3).

It now follows from (3.11) that there exists a subset $I_0 \subset I$ satisfying $|I_0| \geqslant |I|/2$ such that

$$0 \leqslant \chi_i^*(x_0) \leqslant \frac{2\varepsilon}{(3-\tau)n^2} \quad \text{holds for every } i \in I_0. \quad (3.12)$$

Note that in view of (3.6), we have

$$|I_0| \geqslant \frac{(\tau-\varepsilon)n^2}{2}. \quad (3.13)$$

On the other hand, combining (3.7) and (3.12), we see that

$$\lim_{m\to\infty}\frac{1}{m}\sum_{j=0}^{m-1}\chi_i(T^j x_0) = \chi_i^*(x_0) \leqslant \frac{2\varepsilon}{(3-\tau)n^2} \quad \text{holds for every } i \in I_0. \quad (3.14)$$

Since every point in S_0 is *non-pathological*, $T^j x_0$ is well defined for every $j \geqslant 1$. It also follows from (3.14) that there exists a finite threshold m_0 such that for every integer $m \geqslant m_0$,

$$\frac{1}{m}\sum_{j=0}^{m-1}\chi_i(T^j x_0) < \frac{3\varepsilon}{(3-\tau)n^2} \quad \text{holds for every } i \in I_0. \quad (3.15)$$

We recall that χ_i is the characteristic function of the set $S_0 \cap Q_i$. Since x_0 is in the non-trivial T-invariant set S_0, the infinite sequence $T^j x_0$, $j \geqslant 0$, never enters the set $Q_i \setminus S_0$. Let $\chi_i^{\star\star}$ denote the characteristic function of the small n-square Q_i, so that

$$\chi_i^{\star\star}(x) = \begin{cases} 1, & \text{if } x \in Q_i, \\ 0, & \text{otherwise.} \end{cases}$$

Then (3.15) is equivalent to the assertion that for every integer $m \geqslant m_0$,

$$\frac{1}{m}\sum_{j=0}^{m-1}\chi_i^{\star\star}(T^j x_0) < \frac{3\varepsilon}{(3-\tau)n^2} \quad \text{holds for every } i \in I_0. \quad (3.16)$$

Note that every small n-square Q_i has area n^{-2}. Then (3.16) implies that for every integer $m \geqslant m_0$,

$$\sum_{j=0}^{m-1}\chi_i^{\star\star}(T^j x_0) < \frac{9\varepsilon}{(3-\tau)}\frac{\lambda(Q_i)m}{3} \quad \text{holds for every } i \in I_0. \quad (3.17)$$

Choosing a sufficiently small $\varepsilon > 0$, this gives the message that the small n-square Q_i is *grossly undervisited* by the sequence $T^j x_0$, $0 \leqslant j \leqslant m-1$.

Indeed, since $\lambda(X_0) = 3$, the term

$$\frac{\lambda(Q_i)m}{3} = \frac{m}{3n^2} \tag{3.18}$$

represents the *expected value* of the number of the points $T^j x_0 \in Q_i$, $0 \leqslant j \leqslant m-1$. If $0 < \tau < 3$ is fixed and $\varepsilon > 0$ is sufficiently small, then the factor

$$\frac{9\varepsilon}{(3-\tau)}$$

in (3.17) justifies the term *grossly undervisited*. Here we assume that the expected value (3.18) is *large*, which is clearly possible, since $m \geqslant m_0$ can be arbitrarily large.

Note that every Q_i, where $i \in I_0$, is *grossly undervisited*. In view of (3.13), these represent a positive proportion of the total number $3n^2$ of small n-squares in X_0.

Suppose that every small n-square Q_i, $i \in I_0$, is divided into

$$\frac{6\varepsilon m}{(3-\tau)n^2} \tag{3.19}$$

convex parts with equal area; for notational simplicity, let us assume here that the quantity (3.19) is an integer. We refer to these as the *tiny convex parts*. Since

$$\frac{6\varepsilon m}{(3-\tau)n^2} = 2\frac{9\varepsilon}{(3-\tau)}\frac{m}{3n^2},$$

it follows from (3.17) and (3.19) that at least half of these tiny convex parts of Q_i are *empty*, *i.e.*, they do not contain any element of the sequence $T^j x_0$, $0 \leqslant j \leqslant m-1$. We refer to them as the *empty tiny convex parts* of Q_i, $i \in I_0$.

In the next section, we give an explicit construction of these tiny convex parts of Q_i, $i \in I_0$, that have the same area.

4. The magnification process

We consider *iterated area magnification* of convex sets on the faces by using the three X-Y-Z-face hitting properties and the 3-periodicity of the shortline process. We elaborate on this.

Figure 4.1 illustrates area magnification via tilted parallel projection.

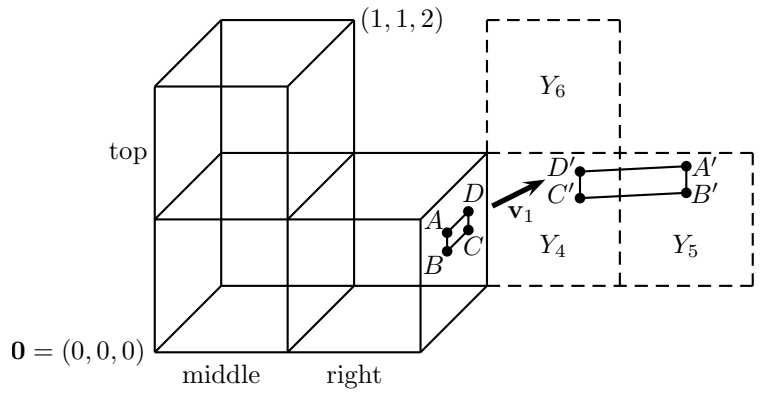

Figure 4.1: magnifying the area via tilted parallel projection

In order to visualize the parallel projection a little better, we have included an extra copy of three unit square faces, indicated by the dashed line squares, on the plane $y = 1$ in cartesian 3-space that can be identified with the square faces Y_4, Y_5, Y_6

of the L-solid. We start with a parallelogram $S_0 = ABCD$ on the square face X_3. Using the $\mathbf{v}_1$-flow indicated by the arrow, where $\mathbf{v}_1 = (1, \alpha_k, \alpha_k^2)$ is the direction vector of the shortline $\mathcal{L}_k^*$ of the geodesic $\mathcal{L}_k$, we project the parallelogram on to the plane $y = 1$. For simplicity, suppose that it is projected on to unit squares identified with $Y_4 \cup Y_5$, as shown. This tilted parallel projection maps the parallelogram S_0 to a new parallelogram $S_1 = A'B'C'D'$, and the area of S_1 is $1/\alpha_k$ times the area of S_0. We say that in Figure 4.1, the image of $S_0 = ABCD$ *splits*, in the sense that the image parallelogram $S_1 = A'B'C'D'$ is located on more than one square face. We aim to avoid splitting as much as possible.

But we do not stop here. We want to describe a full 3-cycle $S_0 \to S_1 \to S_2 \to S_3$ as illustrated in Figure 4.2, where S_2 is on a Z-face and S_3 returns to an X-face.

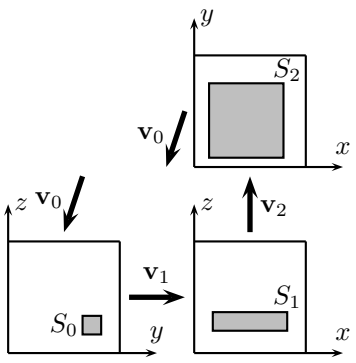

Figure 4.2: illustrating the 3-cycle of the magnification process

In general, we start with a parallelogram S_0 on some square face X_i of the L-solid that is contained in a plane $x = x_0^*$ in cartesian 3-space, where x_0^* is an integer.

As a first step, let us project S_0 by the vector $\mathbf{v}_1 = (1, \alpha_k, \alpha_k^2)$ to a parallelogram S_1 on a plane $y = y_1^*$, where y_1^* is an integer, with the point $(x_0^*, c_1, c_2) \in S_0$ at the center projected to the point $(c_3, y_1^*, c_4) \in S_1$. If $\mathbf{v}_1 = (1, \alpha_k, \alpha_k^2)$ projects a point $(x_0^*, c_1 + y_0, c_2 + z_0) \in S_0$ to the point $(c_3 + x_1, y_1^*, c_4 + z_1) \in S_1$, then simple calculation shows that

$$x_1 = -\frac{y_0}{\alpha_k} = \frac{z_1 - z_0}{\alpha_k^2}.$$

Hence $x_1 = -\alpha_k^{-1} y_0$ and $z_1 = z_0 - \alpha_k y_0$, and so

$$\begin{pmatrix} x_1 \\ z_1 \end{pmatrix} = \begin{pmatrix} -\alpha_k^{-1} & 0 \\ -\alpha_k & 1 \end{pmatrix} \begin{pmatrix} y_0 \\ z_0 \end{pmatrix}. \tag{4.1}$$

As a second step, let us project S_1 by the vector $\mathbf{v}_2 = (\alpha_k^2, 1, \alpha_k)$ to a parallelogram S_2 on a plane $z = z_2^*$, where z_2^* is an integer, with the point $(c_3, y_1^*, c_4) \in S_1$ at the center projected to the point $(c_5, c_6, z_2^*) \in S_2$. If $\mathbf{v}_2 = (\alpha_k^2, 1, \alpha_k)$ projects a point $(c_3 + x_1, y_1^*, c_4 + z_1) \in S_1$ to the point $(c_5 + x_2, c_6 + y_2, z_2^*) \in S_2$, then simple calculation shows that

$$\frac{x_2 - x_1}{\alpha_k^2} = y_2 = -\frac{z_1}{\alpha_k}.$$

Hence $x_2 = x_1 - \alpha_k z_1$ and $y_2 = -\alpha_k^{-1} z_1$, and so

$$\begin{pmatrix} x_2 \\ y_2 \end{pmatrix} = \begin{pmatrix} 1 & -\alpha_k \\ 0 & -\alpha_k^{-1} \end{pmatrix} \begin{pmatrix} x_1 \\ z_1 \end{pmatrix}. \tag{4.2}$$

As a final step, let us project S_2 by the vector $\mathbf{v}_0 = (\alpha_k, \alpha_k^2, 1)$ to a parallelogram S_3 on a plane $x = x_3^*$, where x_3^* is an integer, with the point $(c_5, c_6, z_2^*) \in S_2$ at the center projected to the point $(x_3^*, c_7, c_8) \in S_3$. If $\mathbf{v}_0 = (\alpha_k, \alpha_k^2, 1)$ projects a

point $(c_5 + x_2, c_6 + y_2, z_2^*) \in S_2$ to the point $(x_3^*, c_7 + y_3, c_8 + z_3) \in S_3$, then simple calculation shows that

$$-\frac{x_2}{\alpha_k} = \frac{y_3 - y_2}{\alpha_k^2} = z_3.$$

Hence $y_3 = y_2 - \alpha_k x_2$ and $z_3 = -\alpha_k^{-1} x_2$, and so

$$\begin{pmatrix} y_3 \\ z_3 \end{pmatrix} = \begin{pmatrix} -\alpha_k & 1 \\ -\alpha_k^{-1} & 0 \end{pmatrix} \begin{pmatrix} x_2 \\ y_2 \end{pmatrix}. \tag{4.3}$$

Combining (4.1)–(4.3), we see that this 3-step magnification process has resulted in the transition

$$\begin{pmatrix} y_3 \\ z_3 \end{pmatrix} = \begin{pmatrix} -\alpha_k & 1 \\ -\alpha_k^{-1} & 0 \end{pmatrix} \begin{pmatrix} 1 & -\alpha_k \\ 0 & -\alpha_k^{-1} \end{pmatrix} \begin{pmatrix} -\alpha_k^{-1} & 0 \\ -\alpha_k & 1 \end{pmatrix} \begin{pmatrix} y \\ z \end{pmatrix}.$$

The transition matrix in question is

$$\mathcal{A} = \begin{pmatrix} -\alpha_k & 1 \\ -\alpha_k^{-1} & 0 \end{pmatrix} \begin{pmatrix} 1 & -\alpha_k \\ 0 & -\alpha_k^{-1} \end{pmatrix} \begin{pmatrix} -\alpha_k^{-1} & 0 \\ -\alpha_k & 1 \end{pmatrix} = \begin{pmatrix} 2 - \alpha_k^3 & \alpha_k^2 - \alpha_k^{-1} \\ \alpha_k^{-2} - \alpha_k & 1 \end{pmatrix}.$$

The eigenvalues of this matrix are the roots of the quadratic equation

$$\det \begin{pmatrix} 2 - \alpha_k^3 - \Lambda & \alpha_k^2 - \alpha_k^{-1} \\ \alpha_k^{-2} - \alpha_k & 1 - \Lambda \end{pmatrix} = 0,$$

or $\Lambda^2 - (3 - \alpha_k^3)\Lambda + \alpha_k^{-3} = 0$, with solutions

$$\Lambda_i = \frac{(3 - \alpha_k^3) \pm \mathrm{i}\sqrt{4\alpha_k^{-3} - (3 - \alpha_k^3)^2}}{2}, \quad i = 1, 2, \tag{4.4}$$

and corresponding eigenvectors

$$\mathbf{W}_i = \left(\frac{\Lambda_i - 1}{\alpha_k^{-2} - \alpha_k}, 1 \right), \quad i = 1, 2. \tag{4.5}$$

Note that the two eigenvalues are complex conjugates of each other, as are the first coordinates of the two eigenvectors. It follows that the two vectors

$$\mathbf{u}_1 = \mathbf{W}_1 + \mathbf{W}_2 \quad \text{and} \quad \mathbf{u}_2 = \frac{1}{\mathrm{i}}(\mathbf{W}_1 - \mathbf{W}_2) \tag{4.6}$$

have real coordinates. Indeed, $\mathbf{u}_1 = (u_{1,1}, u_{1,2})$, where

$$u_{1,1} = \frac{2 - \alpha_k^3}{\alpha_k^{-2} - \alpha_k} \quad \text{and} \quad u_{1,2} = 2, \tag{4.7}$$

and $\mathbf{u}_2 = (u_{2,1}, u_{2,2})$, where

$$u_{2,1} = \frac{\sqrt{4\alpha_k^{-3} - (3 - \alpha_k^3)^2}}{\alpha_k^{-2} - \alpha_k} \quad \text{and} \quad u_{2,2} = 0, \tag{4.8}$$

if we ensure that $u_{2,1}$ is positive.

These precise formulas motivate us to start the area magnification process with a small parallelogram S_0 on an X-face that lies on a plane $x = x_0^*$ in cartesian 3-space, and with some very special properties attached to it. Omitting reference to the x-coordinate, we ensure that the non-parallel sides of S_0 are parallel to $\mathbf{u}_1$ and $\mathbf{u}_2$, with lengths respectively

$$\delta|\mathbf{u}_1| = \delta(u_{1,1}^2 + u_{1,2}^2)^{1/2} \quad \text{and} \quad \delta|\mathbf{u}_2| = \delta u_{2,1}, \tag{4.9}$$

where $\delta > 0$ is a small fixed real number.

The 3-step magnification process transforms S_0 into a parallelogram S_3 with the non-parallel sides parallel to the vector

$$\mathbf{u}_1^{(1)} = \mathcal{A}\mathbf{u}_1 = \mathcal{A}(\mathbf{W}_1 + \mathbf{W}_2) = \mathcal{A}\mathbf{W}_1 + \mathcal{A}\mathbf{W}_2 = \Lambda_1\mathbf{W}_1 + \Lambda_2\mathbf{W}_2,$$

with real coordinates and of length

$$\delta|\Lambda_1\mathbf{W}_1 + \Lambda_2\mathbf{W}_2|,$$

and parallel to the vector

$$\mathbf{u}_2^{(1)} = \mathcal{A}\mathbf{u}_2 = \frac{1}{\mathrm{i}}\mathcal{A}(\mathbf{W}_1 - \mathbf{W}_2)r = \frac{1}{\mathrm{i}}(\mathcal{A}\mathbf{W}_1 - \mathcal{A}\mathbf{W}_2) = \frac{1}{\mathrm{i}}(\Lambda_1\mathbf{W}_1 - \Lambda_2\mathbf{W}_2),$$

with real coordinates and of length

$$\delta|\Lambda_1\mathbf{W}_1 - \Lambda_2\mathbf{W}_2|.$$

Indeed, this 3-step magnification process repeated $r \geqslant 1$ times transforms S_0 into a parallelogram S_{3r} on some X-face with the non-parallel sides parallel to the vector

$$\mathbf{u}_1^{(r)} = \Lambda_1^r\mathbf{W}_1 + \Lambda_2^r\mathbf{W}_2, \tag{4.10}$$

with real coordinates and of length

$$\delta|\Lambda_1^r\mathbf{W}_1 + \Lambda_2^r\mathbf{W}_2|, \tag{4.11}$$

and parallel to the vector

$$\mathbf{u}_2^{(r)} = \frac{1}{\mathrm{i}}(\Lambda_1^r\mathbf{W}_1 - \Lambda_2^r\mathbf{W}_2), \tag{4.12}$$

with real coordinates and of length

$$\delta|\Lambda_1^r\mathbf{W}_1 - \Lambda_2^r\mathbf{W}_2|. \tag{4.13}$$

We clearly wish to understand how far the parallelogram S_{3r} differs from the original parallelogram S_0. In particular, we wish to show that it does not look like a long *needle*, with one side substantially longer than the other.

Assume that k is a fixed large integer.

First we estimate the area of S_{3r}. It is clear, since $u_{2,2} = 0$, that

$$\mathrm{area}(S_0) = \delta^2|u_{1,2}||u_{2,1}| = (4 + o_k(1))\delta^2\alpha_k^{1/2}. \tag{4.14}$$

It then follows from the magnification process that

$$\mathrm{area}(S_{3r}) = \alpha_k^{-3r}\,\mathrm{area}(S_0) = (4 + o_k(1))\delta^2\alpha_k^{-3r}\alpha_k^{1/2}. \tag{4.15}$$

Next, we estimate the maximum side length of S_{3r}. Note first of all that it clearly follows from (4.4) that

$$|\Lambda_i| = \alpha_k^{-3/2}, \quad i = 1, 2.$$

Combining this with (4.5), we see that

$$|\mathbf{W}_i| \leqslant 2, \quad i = 1, 2.$$

It follows, on noting that the side lengths of S_{3r} are given by (4.11) and (4.13), that the maximum side length of S_{3r} satisfies

$$\text{max-sidelength}(S_{3r}) \leqslant \delta(|\Lambda_1|^r|\mathbf{W}_1| + |\Lambda_2|^r|\mathbf{W}_2|) \leqslant 4\delta\alpha_k^{-3r/2}. \tag{4.16}$$

Combining (4.15) and (4.16), we deduce that

$$\frac{(\text{max-sidelength}(S_{3r}))^2}{\mathrm{area}(S_{3r})} \leqslant \frac{4 + o_k(1)}{\alpha_k^{1/2}}. \tag{4.17}$$

This shows that uniformly S_{3r} does not look like a long needle.

Recall that towards the end of the previous section, we wish to divide each small n-square Q_i, $i \in I_0$, into

$$\frac{6\varepsilon m}{(3-\tau)n^2} \tag{4.18}$$

convex parts with equal area, referred to as the *tiny convex parts*, and that for notational simplicity, we assume that the quantity (4.18) is an integer. Recall also that at least half of these tiny convex parts of Q_i do not contain any element of the sequence $T^j x_0$, $0 \leqslant j \leqslant m-1$, and that we refer to them as the *empty tiny convex parts* of Q_i, $i \in I_0$. Now we are ready to give the explicit construction.

Since every empty tiny convex part of Q_i, $i \in I_0$, has relatively large area, we can employ the area magnification process on any of them. Of course the magnified image of an *empty* set is also *empty*. We shall show that there exists at least one such empty tiny convex part of some Q_i, $i \in I_0$, which avoids *image-splitting* during the *entire* area magnification process.

We define the *tiny convex parts* as congruent parallelograms on an X-face such that one side is parallel to $\mathbf{u}_1$ with length $\delta|\mathbf{u}_1|$, and the other side is parallel to $\mathbf{u}_2$ with length $\delta|\mathbf{u}_2|$; see (4.5)–(4.9). Thus we consider a parallelogram lattice

$$\Omega = \Omega(\mathbf{u}_1, \mathbf{u}_2; \delta) \tag{4.19}$$

on the plane, where any fundamental parallelogram $\mathcal{P} \in \Omega$, an atoms of Ω, has sides $\delta\mathbf{u}_1$ and $\delta\mathbf{u}_2$. The concrete value of the parameter $\delta > 0$ will be specified later.

It is a minor irritation that the parallelogram lattice Ω in (4.19) may not tile a unit size square precisely. However, we shall show later that, with an appropriate choice of the parameters, this technical issue has a totally negligible effect.

The whole magnification process consists of a large number of consecutive 3-cycles. It makes the calculations more convenient if we write the total number of consecutive 3-cycles as $\ell - O(1)$, where the value of the constant $O(1)$ will be specified later.

We choose the parameters δ and ℓ such that

$$\delta|\Lambda_1^\ell| = \delta|\Lambda_2^\ell| = \delta\alpha_k^{-3\ell/2} \asymp 1. \tag{4.20}$$

This will be made more precise later.

The area of any fundamental parallelogram in the lattice $\Omega = \Omega(\mathbf{u}_1, \mathbf{u}_2; \delta)$ defined in (4.19) is chosen to be precisely equal to $(3-\tau)/6\varepsilon m$. Combining this with (4.14), the area of any fundamental parallelogram in the lattice $\Omega = \Omega(\mathbf{u}_1, \mathbf{u}_2; \delta)$ is equal to

$$(4 + o_k(1))\delta^2\alpha_k^{1/2} = \frac{3-\tau}{6\varepsilon m}. \tag{4.21}$$

Since the area of an arbitrary small n-square Q_i, $i \in I_0$, is equal to n^{-2}, it follows that the number of the fundamental parallelograms $\mathcal{P}$ in $\Omega = \Omega(\mathbf{u}_1, \mathbf{u}_2; \delta)$ that intersect Q_i is between $5\varepsilon m/(3-\tau)n^2$ and $7\varepsilon m/(3-\tau)n^2$, where the number would be precisely $6\varepsilon m/(3-\tau)n^2$ in the case of perfect tiling, assuming that m is sufficiently large.

We now take the fundamental parallelograms $\mathcal{P}$ of $\Omega = \Omega(\mathbf{u}_1, \mathbf{u}_2; \delta)$ in Q_i as the tiny convex parts mentioned above. Then it follows that there are at least

$$\frac{5\varepsilon m}{(3-\tau)n^2} = \frac{5}{3}\frac{9\varepsilon}{(3-\tau)}\frac{m}{3n^2}$$

fundamental parallelograms in Q_i. It then follows from (3.17) that a proportion of at least $1 - (3/5) = 2/5$ of the fundamental parallelograms $\mathcal{P}$ in Q_i are empty, *i.e.*,

they do not contain any element of the sequence $T^j x_0$, $0 \leqslant j \leqslant m-1$. We refer to them as the *empty fundamental parallelograms* $\mathcal{P}$ in Q_i, $i \in I_0$. There are at least

$$\frac{2\varepsilon m}{(3-\tau)n^2}$$

of them. Combining this with (3.13), there are at least

$$\frac{(\tau-\varepsilon)n^2}{2}\frac{2\varepsilon m}{(3-\tau)n^2} = \frac{\varepsilon(\tau-\varepsilon)m}{3-\tau} \tag{4.22}$$

empty fundamental parallelograms $\mathcal{P}$ in X_0.

Since $\lambda(X_0) = 3$, noting that the area of a fundamental parallelogram is given by (4.21), there are

$$\frac{3}{\frac{3-\tau}{6\varepsilon m}} \pm \varepsilon^2 m = \left(\frac{18\varepsilon}{3-\tau} \pm \varepsilon^2\right) m \tag{4.23}$$

fundamental parallelograms of the lattice $\Omega = \Omega(\mathbf{u}_1, \mathbf{u}_2; \delta)$ in X_0, assuming m is large enough. Here, the error term $\pm\varepsilon^2 m$ comes from the contribution near the border.

Comparing (4.22) and (4.23), we conclude that the ratio of empty fundamental parallelograms $\mathcal{P}$ in X_0 compared to the total number in X_0 is at least

$$\frac{\tau-\varepsilon}{20}, \tag{4.24}$$

assuming that $\varepsilon > 0$ is sufficiently small.

Our basic idea is that each such grossly undervisited small n-square Q_i has many pairwise disjoint convex *empty* sets $\mathcal{P} \in \Omega = \Omega(\mathbf{u}_1, \mathbf{u}_2; \delta)$ with the same non-negligible area, for which we can apply the area magnification process via shortlines. In the magnification process, we work with the concrete half-infinite geodesic that starts from the special point $x_0 \in S_0$, and of course we use its shortlines.

We want to avoid the annoying technical problem of image-splitting illustrated in Figure 4.1. Since there are many candidates for convex *empty* sets, we have a good chance of showing that *at least one of them* is *splitting-free* in the precise sense that it never splits during the entire magnification process.

The details of the magnification process are rather complicated, and the reader may wish to jump ahead right now and read the conclusion of Section 5 summarized in the last paragraph of the section and then Section 6. This is the quickest way to get a rough idea on how the proof works. After that the reader can come back to Section 5 and study the technical details of the magnification process.

Let $1 \leqslant r \leqslant \ell$ be an arbitrary integer. We use r as a running parameter to describe a general 3-cycle in the magnification process of $\ell - O(1)$ consecutive 3-cycles.

Starting from a fundamental parallelogram $\mathcal{P}$ of $\Omega(\mathbf{u}_1, \mathbf{u}_2; \delta)$, and carrying out r consecutive 3-cycles of the area magnification process via shortlines, we obtain a new parallelogram $\mathcal{P}^{(r)}$ on an X-face, or X-faces, such that one side is the vector $\delta\mathbf{u}_1^{(r)}$, and the other side is the vector $\delta\mathbf{u}_2^{(r)}$; see (4.10)–(4.13).

Of course, we are particularly interested in empty fundamental parallelograms $\mathcal{P} \in \Omega(\mathbf{u}_1, \mathbf{u}_2; \delta)$.

5. Grids and iteration

We first establish the following geometric result that we shall use a few times.

Lemma 5.1 ("area lemma"). *Let Ω be an arbitrary parallelogram lattice in $\mathbb{R}^2$ such that each fundamental parallelogram has diameter $\eta > 0$ and area Δ. Then a straight line segment S with length $L > 0$ intersects at most*

$$\frac{2\eta(L+2\eta)}{\Delta}$$

fundamental parallelograms in Ω.

Proof. For any two points $P, Q \in \mathbb{R}^2$, let $\rho(P,Q)$ denote the usual euclidean distance between P and Q. For any $\eta > 0$, consider the η-neighborhood of S given by

$$S(\eta) = \{P \in \mathbb{R}^2 : \rho(P,Q) \leqslant \eta \text{ for some } Q \in S\}.$$

It is easy to see that $\text{area}(S(\eta)) \leqslant 2\eta(L+2\eta)$. Note next that every fundamental parallelogram in Ω that intersects S is completely contained in $S(\eta)$. Since each such fundamental parallelogram has area Δ, a simple calculation shows that the number of fundamental parallelograms in Ω that intersect S does not exceed

$$\frac{\text{area}(S(\eta))}{\Delta} \leqslant \frac{2\eta(L+2\eta)}{\Delta}.$$

This completes the proof. □

Throughout, we assume that $k \geqslant 8$, so that $\alpha_k < 1/16$.

We need some notation.

First of all, we rewrite (4.20) in the form

$$\delta = \frac{\alpha_k^{3\ell/2}}{c_1}, \tag{5.1}$$

where the constant $c_1 > 0$ will be specified later. We also write

$$\ell = r + (r-1) + (r-2) + \ldots + c_2 = \frac{r(r+1)}{2} - \frac{(c_2-1)c_2}{2},$$

where the constant $c_2 \geqslant 10$ will be specified later. More generally, for every integer $i = 0, 1, 2, \ldots, r - c_2$, we write

$$\ell_i = \sum_{h=0}^{i}(r-h) = \frac{r(r+1)}{2} - \frac{(r-i-1)(r-i)}{2}, \tag{5.2}$$

so that in particular

$$\ell_0 = r, \quad \ell_1 = r + (r-1), \quad \ell_{r-c_2-1} = \ell - c_2 \quad \text{and} \quad \ell_{r-c_2} = \ell, \tag{5.3}$$

and let the integer q_i satisfy the inequalities

$$\frac{c_1}{(r-i)^4}\alpha_k^{-3(\ell-\ell_i)/2} - 1 < q_i \leqslant \frac{c_1}{(r-i)^4}\alpha_k^{-3(\ell-\ell_i)/2}. \tag{5.4}$$

In particular, the integer $q = q_0$ satisfies the inequalities

$$\frac{c_1}{r^4}\alpha_k^{-3(\ell-r)/2} - 1 < q \leqslant \frac{c_1}{r^4}\alpha_k^{-3(\ell-r)/2}. \tag{5.5}$$

The calculations here and below makes use of the key fact that we can choose the value of the parameter ℓ as large as possible. It follows that $r \approx \sqrt{2\ell}$ can also be arbitrarily large.

We are now ready to describe an iterative process that allows us to construct *grids* that contain *empty* fundamental parallelograms that are also *non-splitting* during the magnification process.

Preparatory Step. We begin our process with a $q \times q$ grid $\mathcal{G}$ of fundamental parallelograms $\mathcal{P} \in \Omega$. Since each fundamental parallelogram $\mathcal{P} \in \Omega$ has sides given by the vectors $\delta\mathbf{u}_1$ and $\delta\mathbf{u}_2$, a $q \times q$ grid $\mathcal{G}$ consists of q^2 fundamental parallelograms $\mathcal{P} \in \Omega$ and is itself a larger parallelogram with sides given by the vectors $q\delta\mathbf{u}_1$ and $q\delta\mathbf{u}_2$.

Consider a parallelogram lattice $\mathcal{H}$ that contains an X-face, with grid fundamental parallelograms given by $q \times q$ grids $\mathcal{G}$ with sides given by the vectors $q\delta\mathbf{u}_1$ and $q\delta\mathbf{u}_2$.

Remark. Here we use the term grid fundamental parallelograms to distinguish these larger parallelograms from the fundamental parallelograms $\mathcal{P} \in \Omega$.

It follows easily from (4.7)–(4.9) that the diameter of each grid fundamental parallelogram in $\mathcal{H}$ does not exceed

$$8q\delta \leqslant \frac{8\alpha_k^{3r/2}}{r^4} \leqslant \frac{1}{2r^4}, \tag{5.6}$$

in view of (5.1), (5.5) and the assumption on k. This is extremely small when r is large, and ensures that there are many $q \times q$ grids $\mathcal{G}$ that are completely contained in an X-face of X_0. It also follows easily from (4.14) that each grid fundamental parallelogram in $\mathcal{H}$ has area $\Delta = (4+o_k(1))q^2\delta^2\alpha_k^{1/2}$. On the other hand, an X-face has 4 boundary edges, each with unit length. Applying Lemma 5.1, we conclude that the number of grid fundamental parallelograms in $\mathcal{H}$ that intersect the boundary of any of the 3 X-faces in X_0 does not exceed

$$3 \cdot 4 \cdot \frac{16q\delta(1+16q\delta)}{(4+o_k(1))q^2\delta^2\alpha_k^{1/2}} = \frac{48+o_k(1)}{q\delta\alpha_k^{1/2}}.$$

The total number of fundamental parallelograms $\mathcal{P} \in \Omega$ is roughly equal to

$$\frac{3q^2}{(4+o_k(1))q^2\delta^2\alpha_k^{1/2}},$$

so it follows from (4.24) and (5.6) that the total number of empty fundamental parallelograms $\mathcal{P} \in \Omega$ contained in $q \times q$ grids $\mathcal{G}$ that do not intersect the boundary of any of the 3 X-faces in X_0 is at least

$$\begin{aligned}&\frac{3q^2}{(4+o_k(1))q^2\delta^2\alpha_k^{1/2}} \cdot \frac{\tau-\varepsilon}{20} - \frac{(48+o_k(1))q^2}{q\delta\alpha_k^{1/2}}\\ &\quad = \frac{3}{(4+o_k(1))q^2\delta^2\alpha_k^{1/2}}\left(\frac{\tau-\varepsilon}{20} - (48+o_k(1))q\delta\right)q^2.\end{aligned}$$

Thus the average proportion of empty fundamental parallelograms in a $q \times q$ grid $\mathcal{G}$ that does not intersect the boundary of any of the 3 X-faces in X_0 is at least

$$\frac{\tau-\varepsilon}{20} - (48+o_k(1))q\delta.$$

Note that it follows from (5.6) that

$$(48+o_k(1))q\delta \leqslant \frac{3}{r^4} < \frac{\tau}{100r^2}$$

for large r.

We now choose a $q \times q$ grid $\mathcal{G}_0$ that is completely contained in an X-face of X_0 and contains the maximum number of empty fundamental parallelograms $\mathcal{P} \in \Omega$.

Clearly the proportion of empty fundamental parallelograms $\mathcal{P} \in \mathcal{G}_0$ is at least

$$\tau_0 = \frac{\tau - \varepsilon}{20} - \frac{\tau}{100r^2}. \tag{5.7}$$

Initial Step. Starting with $\mathcal{G}_0$ and applying the first 3-cycle of magnifications

$$X_0 \xrightarrow{\mathbf{v}_1} Y_0 \xrightarrow{\mathbf{v}_2} Z_0 \xrightarrow{\mathbf{v}_0} X_0,$$

where

$$Y_0 = Y_1 \cup Y_2 \cup Y_3 \quad \text{and} \quad Z_0 = Z_1 \cup Z_2 \cup Z_5$$

as shown in Figures 2.2 and 2.3, we obtain a magnified $q \times q$ grid $\mathcal{G}_0^{(1)}$. Performing this argument r times successively, we obtain a magnified $q \times q$ grid $\mathcal{G}_0^{(r)} = \mathcal{G}_0^{(\ell_0)}$ at the end of r consecutive 3-cycles of magnifications. At each magnification, the diameter of the parallelogram grows by a factor $\alpha_k^{-1/2}$, so that the diameter of the parallelogram at each stage of the $3r$-step magnification process, assuming that no splitting takes place, never exceeds

$$8q\delta\alpha_k^{-3r/2} \leqslant \frac{8}{r^4} \leqslant 1, \tag{5.8}$$

in view of (5.6), as long as $r \geqslant 2$. If splitting occurs at any step of the magnification process, the bound (5.8) on the diameter guarantees that the image splits into at most 4 convex parts, each contained in a square face. For convenience, we call these *convex square-parts*.

Remark. Note that the L-solid has only 14 square faces in total. This number is reduced to 9 with face identification. Thus many distinct convex square-parts may fall into the same square face. However, we need to exercise care and treat each separately.

Since there are $3r$ steps in the magnification process, it follows that the $q \times q$ grid $\mathcal{G}_0^{(r)}$ splits into $R \leqslant 4^{3r}$ convex square-parts.

Let A be a convex square-part of $\mathcal{G}_0^{(r)}$, and suppose that it is contained in the unit square face U.

Suppose first of all that A contains a vertex P_0 of $\mathcal{G}_0^{(r)}$. We consider a parallelogram lattice $\mathcal{H}_0$, where P_0 is one of the vertices and a grid fundamental parallelogram in $\mathcal{H}_0$ has sides given by the vectors $q_1\delta\mathbf{u}_1^{(r)}$ and $q_1\delta\mathbf{u}_2^{(r)}$. We say that a grid fundamental parallelogram in $\mathcal{H}_0$ is *good* if it is completely inside A, and *bad* if it intersects the boundary of A. Those grid fundamental parallelograms that do not intersect A are *irrelevant* to our discussion.

The convex square-part A of $\mathcal{G}_0^{(r)}$ is the intersection of a parallelogram with the unit square face U, and therefore has at most 8 straight edges, each of length at most $L = \sqrt{2}$. Meanwhile, it follows from (4.16) that the diameter η of each grid fundamental parallelogram in $\mathcal{H}_0$ satisfies

$$\eta \leqslant 8q_1\delta\alpha_k^{-3r/2},$$

and it follows from (4.15) that each grid fundamental parallelogram in $\mathcal{H}_0$ has area

$$\Delta = (4 + o_k(1))q_1^2\delta^2\alpha_k^{-3r}\alpha_k^{1/2}.$$

Applying Lemma 5.1, we conclude that there are at most

$$8 \cdot \frac{16q_1\delta\alpha_k^{-3r/2}(\sqrt{2} + 16q_1\delta\alpha_k^{-3r/2})}{(4 + o_k(1))q_1^2\delta^2\alpha_k^{-3r}\alpha_k^{1/2}} \leqslant \frac{64 + o_k(1)}{q_1\delta\alpha_k^{-3r/2}\alpha_k^{1/2}} \tag{5.9}$$

bad grid fundamental parallelograms in $\mathcal{H}_0$ that intersect the convex square-part A of $\mathcal{G}_0^{(r)}$.

Suppose next that A does not contain a vertex P_0 of $\mathcal{G}_0^{(r)}$. Then A is *small*, and we can consider an arbitrary parallelogram lattice $\mathcal{H}_0$ with sides given by the vectors $q_1\delta\mathbf{u}_1^{(r)}$ and $q_1\delta\mathbf{u}_2^{(r)}$. An analogous argument shows that the estimate (5.9) remains valid.

There are at most 4^{3r} convex square-parts of $\mathcal{G}_0^{(r)}$. It follows that the total number of bad grid fundamental parallelograms that intersect any convex square-part of $\mathcal{G}_0^{(r)}$ is at most

$$4^{3r} \cdot \frac{64 + o_k(1)}{q_1\delta\alpha_k^{-3r/2}\alpha_k^{1/2}},$$

and so the total number of fundamental parallelograms $\mathcal{P}^{(r)} \in \mathcal{G}_0^{(r)}$ contained in bad grid fundamental parallelograms in $\mathcal{G}_0^{(r)}$ is at most

$$4^{3r} \cdot \frac{(64 + o_k(1))q_1^2}{q_1\delta\alpha_k^{-3r/2}\alpha_k^{1/2}}.$$

Now the total number of fundamental parallelograms $\mathcal{P}^{(r)} \in \mathcal{G}_0^{(r)}$ is equal to q^2. On the other hand, since the magnified image of an empty set is empty, the proportion of empty fundamental parallelograms $\mathcal{P}^{(r)} \in \mathcal{G}_0^{(r)}$ is at least τ_0 given by (5.7). Hence the total number of empty fundamental parallelograms $\mathcal{P}^{(r)} \in \mathcal{G}_0^{(r)}$ contained in good grid fundamental parallelograms in $\mathcal{G}_0^{(r)}$ is at least

$$q^2\tau_0 - 4^{3r} \cdot \frac{(64 + o_k(1))q_1^2}{q_1\delta\alpha_k^{-3r/2}\alpha_k^{1/2}}.$$

Thus the average proportion of empty fundamental parallelograms in a good $q_1 \times q_1$ grid fundamental parallelogram in $\mathcal{G}_0^{(r)}$ is at least

$$\tau_0 - \frac{4^{3r}}{q^2} \cdot \frac{(64 + o_k(1))q_1^2}{q_1\delta\alpha_k^{-3r/2}\alpha_k^{1/2}}.$$

Note that it follows from (5.1) and (5.3)–(5.5) that

$$\frac{4^{3r}}{q^2} \cdot \frac{(64 + o_k(1))q_1^2}{q_1\delta\alpha_k^{-3r/2}\alpha_k^{1/2}} = \frac{(64 + o_k(1))}{(r-1)^4}\alpha_k^{-2}(4\alpha_k^{1/2})^{3r}r^8 < \frac{\tau}{100(r-1)^2}$$

for large r.

We now choose a $q_1 \times q_1$ grid $\mathcal{G}_1$ which is a good grid fundamental parallelogram in $\mathcal{G}_0^{(\ell_0)} = \mathcal{G}_0^{(r)}$ and which contains the maximum number of empty fundamental parallelograms $\mathcal{P}^{(\ell_0)} = \mathcal{P}^{(r)}$ which are images of $\mathcal{P} \in \mathcal{G}_0$. Clearly the proportion of empty fundamental parallelograms $\mathcal{P}^{(\ell_0)} = \mathcal{P}^{(r)} \in \mathcal{G}_1$ is at least

$$\tau_1 = \tau_0 - \frac{\tau}{100(r-1)^2}. \tag{5.10}$$

Furthermore, since the image $\mathcal{P}^{(\ell_0)} = \mathcal{P}^{(r)}$ of the fundamental parallelogram $\mathcal{P}$ under the $3\ell_0 = 3r$ magnifications is completely inside a convex square-part of $\mathcal{G}_0^{(\ell_0)} = \mathcal{G}_0^{(r)}$, $\mathcal{P}$ never splits during the $3\ell_0 = 3r$ magnifications. In particular, these empty fundamental parallelograms are non-splitting.

Inductive Step. Suppose, in general, that $\mathcal{G}_i$ is $q_i \times q_i$ grid which is a good grid fundamental parallelogram, contained in a convex square-part of $\mathcal{G}_0^{(\ell_{i-1})} = \mathcal{G}_{i-1}^{(r-i+1)}$,

and that the proportion of empty and non-splitting fundamental parallelograms $\mathcal{P}^{(\ell_{i-1})} \in \mathcal{G}_i$ is at least

$$\tau_i = \tau_{i-1} - \frac{\tau}{100(r-i)^2}, \tag{5.11}$$

where $\mathcal{P}^{(\ell_{i-1})}$ represents the image of $\mathcal{P}$ under $3\ell_{i-1}$ magnifications, remaining empty and non-splitting during the entire process $\mathcal{G}_0 \to \mathcal{G}_i$.

Starting with $\mathcal{G}_i$ and applying the first 3-cycle of magnifications

$$X_0 \xrightarrow{\mathbf{v}_1} Y_0 \xrightarrow{\mathbf{v}_2} Z_0 \xrightarrow{\mathbf{v}_0} X_0,$$

we now obtain a magnified $q_i \times q_i$ grid $\mathcal{G}_i^{(1)}$. Performing this argument $r-i$ times successively, we obtain a magnified $q_i \times q_i$ grid $\mathcal{G}_i^{(r-1)} = \mathcal{G}_0^{(\ell_i)}$ at the end of $r-i$ consecutive 3-cycles of magnifications. The diameter of the grid $\mathcal{G}_i$ is clearly bounded by $8q_i\delta\alpha_k^{-3\ell_{i-1}/2}$. At each magnification, the diameter of the parallelogram grows by a factor $\alpha_k^{-1/2}$, so that the diameter of the parallelogram at each stage of the present $3(r-i)$-step magnification process, assuming that no splitting takes place, never exceeds

$$8q_i\delta\alpha_k^{-3\ell_{i-1}/2}\alpha_k^{-3(r-i)/2} = 8q_i\delta\alpha_k^{-3\ell_i/2} \leqslant \frac{8}{(r-i)^4} \leqslant 1, \tag{5.12}$$

in view of (5.1) and (5.4), as long as $r-i \geqslant 2$. If splitting occurs at any step of the magnification process, the bound (5.12) on the diameter guarantees that the image splits into at most 4 convex square-parts, each contained in a square face. Since there are $3(r-i)$ steps in the magnification process, it follows that the $q_i \times q_i$ grid $\mathcal{G}_i^{(r-i)}$ splits into $R_i \leqslant 4^{3(r-i)}$ convex square-parts.

Let A be a convex square-part of $\mathcal{G}_i^{(r-i)}$, and suppose that it is contained in the unit square face U. We may suppose that A contains a vertex P_0 of $\mathcal{G}_0^{(r)}$, as the argument in the alternative case requires only minor modifications. We consider a parallelogram lattice $\mathcal{H}_i$, where P_0 is one of the vertices and a grid fundamental parallelogram in $\mathcal{H}_i$ has sides given by the vectors $q_{i+1}\delta\mathbf{u}_1^{(\ell_i)}$ and $q_{i+1}\delta\mathbf{u}_2^{(\ell_i)}$. We say that a grid fundamental parallelogram in $\mathcal{H}_i$ is *good* if it is completely inside A, and *bad* if it intersects the boundary of A. Those grid fundamental parallelograms that do not intersect A are *irrelevant* to our discussion.

The convex square-part A of $\mathcal{G}_i^{(r-i)}$ is the intersection of a parallelogram with the unit square face U, and therefore has at most 8 straight edges, each of length at most $L = \sqrt{2}$. Meanwhile, it follows from (4.16) that the diameter η of each grid fundamental parallelogram in $\mathcal{H}_i$ satisfies

$$\eta \leqslant 8q_{i+1}\delta\alpha_k^{-3\ell_i/2},$$

and it follows from (4.15) that each grid fundamental parallelogram in $\mathcal{H}_0^{(r)}$ has area

$$\Delta = (4 + o_k(1))q_{i+1}^2\delta^2\alpha_k^{-3\ell_i}\alpha_k^{1/2}.$$

Applying Lemma 5.1, we conclude that there are at most

$$8 \cdot \frac{16q_{i+1}\delta\alpha_k^{-3\ell_i/2}(\sqrt{2} + 16q_{i+1}\delta\alpha_k^{-3\ell_i/2})}{(4 + o_k(1))q_{i+1}^2\delta^2\alpha_k^{-3\ell_i}\alpha_k^{1/2}} \leqslant \frac{64 + o_k(1)}{q_{i+1}\delta\alpha_k^{-3\ell_i/2}\alpha_k^{1/2}}$$

bad grid fundamental parallelograms in $\mathcal{H}_i$ that intersect the convex square-part A of $\mathcal{G}_i^{(r-i)}$.

There are at most $4^{3(r-i)}$ convex square-parts of $\mathcal{G}_i^{(r-i)}$. It follows that the total number of bad grid fundamental parallelograms that intersect any convex square-part of $\mathcal{G}_i^{(r-i)}$ is at most

$$4^{3(r-i)} \cdot \frac{64 + o_k(1)}{q_{i+1}\delta\alpha_k^{-3\ell_i/2}\alpha_k^{1/2}},$$

and so the total number of fundamental parallelograms $\mathcal{P}^{(\ell_i)} \in \mathcal{G}_i^{(r-i)}$ contained in bad grid fundamental parallelograms in $\mathcal{G}_i^{(r-i)}$ is at most

$$4^{3(r-i)} \cdot \frac{(64 + o_k(1))q_{i+1}^2}{q_{i+1}\delta\alpha_k^{-3\ell_i/2}\alpha_k^{1/2}}.$$

Now the total number of fundamental parallelograms $\mathcal{P}^{(\ell_i)} \in \mathcal{G}_i^{(r-i)}$ is equal to q_i^2. On the other hand, since the magnified image of an empty set is empty, the proportion of empty fundamental parallelograms $\mathcal{P}^{(\ell_i)} \in \mathcal{G}_i^{(r-i)}$ is at least τ_i given by (5.11). Hence the total number of empty fundamental parallelograms $\mathcal{P}^{(\ell_i)} \in \mathcal{G}_i^{(r-i)}$ contained in good grid fundamental parallelograms in $\mathcal{G}_i^{(r-i)}$ is at least

$$q_i^2\tau_i - 4^{3(r-i)} \cdot \frac{(64 + o_k(1))q_{i+1}^2}{q_{i+1}\delta\alpha_k^{-3\ell_i/2}\alpha_k^{1/2}}.$$

It follows that the average proportion of empty fundamental parallelograms in a good $q_{i+1} \times q_{i+1}$ grid fundamental parallelogram in $\mathcal{G}_i^{(r-i)}$ is at least

$$\tau_i - \frac{4^{3(r-i)}}{q_i^2} \cdot \frac{(64 + o_k(1))q_{i+1}^2}{q_{i+1}\delta\alpha_k^{-3\ell_i/2}\alpha_k^{1/2}}.$$

Note that it follows from (5.1), (5.2) and (5.4) that

$$\frac{4^{3(r-i)}}{q_i^2} \cdot \frac{(64 + o_k(1))q_{i+1}^2}{q_{i+1}\delta\alpha_k^{-3\ell_i/2}\alpha_k^{1/2}} = \frac{(64 + o_k(1))}{(r-i-1)^4}\alpha_k^{-2}(4\alpha_k^{1/2})^{3(r-i)}(r-i)^8 < \frac{\tau}{100(r-i-1)^2}$$

for large $r - i$. Since $r - i \geqslant c_2$, we can choose c_2 sufficiently large so that

$$\alpha_k^{-2}(4\alpha_k^{1/2})^{3(r-i)}(r-i)^8 \leqslant 1$$

whenever $r - i \geqslant c_2$, for instance.

We can now choose a $q_{i+1} \times q_{i+1}$ grid $\mathcal{G}_{i+1}$ which is a good grid fundamental parallelogram in $\mathcal{G}_0^{(\ell_i)} = \mathcal{G}_i^{(r-i)}$ and which contains the maximum number of empty fundamental parallelograms $\mathcal{P}^{(\ell_i)}$ which are images of $\mathcal{P} \in \mathcal{G}_0$. Clearly the proportion of empty fundamental parallelograms $\mathcal{P}^{(\ell_i)} \in \mathcal{G}_{i+1}$ is at least

$$\tau_{i+1} = \tau_i - \frac{\tau}{100(r-i-1)^2}.$$

Furthermore, since the image $\mathcal{P}^{(\ell_i)}$ of the fundamental parallelogram $\mathcal{P}$ under the $3\ell_i$ magnifications is completely inside a convex square-part of $\mathcal{G}_0^{(\ell_i)} = \mathcal{G}_i^{(r-i)}$, $\mathcal{P}$ never splits during the $3\ell_i$ magnifications from the very beginning. In particular, these empty fundamental parallelograms are non-splitting.

Last Step. The final step of this iterative process concerns $i = r - c_2 - 1$, with $\ell_i = \ell - c_2$. We conclude that we can choose an $(r - c_2) \times (r - c_2)$ grid $\mathcal{G}_{r-c_2}$ which is a good grid fundamental parallelogram in $\mathcal{G}_0^{(\ell-c_2)} = \mathcal{G}_{r-c_2-1}^{(c_2+1)}$, and the proportion of empty and parallelograms $\mathcal{P}^{(\ell-c_2)} \in \mathcal{G}_{r-c_2}$ is at least

$$\tau_{r-c_2} = \tau_{r-c_2-1} - \frac{\tau}{100c_2^2}. \tag{5.13}$$

Furthermore, since the image $\mathcal{P}^{(\ell-c_2)}$ of the fundamental parallelogram $\mathcal{P}$ under the $3(\ell-c_2)$ magnifications is completely inside a convex square-part of $\mathcal{G}_0^{(\ell-c_2)}$, $\mathcal{P}$ never splits during the $3(\ell-c_2)$ magnifications from the very beginning. In particular, these empty fundamental parallelograms are non-splitting.

Combining (5.7), (5.10), (5.11) and (5.13), we see that

$$\tau_{r-c_2} = \frac{\tau-\varepsilon}{20} - \frac{\tau}{100}\sum_{h=c_2}^{r}\frac{1}{h^2} > \frac{\tau-\varepsilon}{20} - \frac{\tau}{50} > \frac{\tau-2\varepsilon}{40} > 0$$

if $\varepsilon < \tau/2$. Note also from (5.3) and (5.4) that

$$q_{r-c_2} > \frac{c_1}{c_2^4} - 1 = 1$$

if we specify that $c_1 = 2c_2^4$.

Thus we have shown that there exists an empty parallelogram $\mathcal{P}_0 \in \Omega$ such that the $3(\ell-c_2)$-step magnification process gives rise to an empty parallelogram $\mathcal{P}_0^{(\ell-c_2)}$, and there is no splitting during the entire process of $\ell - c_2$ consecutive 3-cycles of magnifications.

6. Conclusion via Time-quantitative Density B

As discussed in Sections 2–3, the magnification process begins with a particular geodesic segment starting from the special point $x_0 \in S_0$ satisfying (3.11) and which subsequently hits the X-faces at the points $T^j x_0$, $0 \leqslant j \leqslant m-1$, where the parameter m will be chosen to be large but is as yet unspecified. This gives rise to a union $\mathcal{L}_k(0)$ of m consecutive *shortcuts*, each of length $(1+\alpha_k^2+\alpha_k^4)^{1/2}$, and so

$$\text{length}(\mathcal{L}_k(0)) = m(1+\alpha_k^2+\alpha_k^4)^{1/2}.$$

The $3(\ell-c_2)$ area magnifications are carried out by $3(\ell-c_2)$ consecutive steps of the iterated shortline process, starting with $\mathcal{L}_k(0)$. Formally, we have the sequence

$$\mathcal{L}_k(0) \to \mathcal{L}_k(1) \to \mathcal{L}_k(2) \to \ldots \to \mathcal{L}_k(3(\ell-c_2))$$

of shortline segments of decreasing length, where $\to$ denotes the shortline operation. We know from [1, Section 6.3] that

$$\text{length}(\mathcal{L}_k(i)) = \alpha_k^i \,\text{length}(\mathcal{L}_k(0))$$

for every $1 \leqslant i \leqslant 3(\ell-c_2)$. Thus

$$\text{length}(\mathcal{L}_k(3(\ell-c_2))) = \alpha_k^{3(\ell-c_2)} \,\text{length}(\mathcal{L}_k(0)) = \alpha_k^{3(\ell-c_2)} m(1+\alpha_k^2+\alpha_k^4)^{1/2}. \quad (6.1)$$

We recall (4.14), (4.21) and (5.1), that the area of any fundamental parallelogram $\mathcal{P} \in \Omega = \Omega(\mathbf{u}_1, \mathbf{u}_2; \delta)$ is equal to

$$(4+o_k(1))\delta^2\alpha_k^{1/2} = \frac{(4+o_k(1))\alpha_k^{3\ell}\alpha_k^{1/2}}{c_1^2} \approx \frac{3-\tau}{6\varepsilon m}.$$

Note that

$$\alpha_k^{3\ell} m \approx \frac{(3-\tau)c_1^2}{\varepsilon(24+o_k(1))\alpha_k^{1/2}}. \quad (6.2)$$

Combining this with (6.1), we obtain

$$\text{length}(\mathcal{L}_k(3(\ell-c_2))) = \frac{c_3}{\varepsilon}, \quad (6.3)$$

where $c_3 = c_3(\alpha_k; \tau; c_1, c_2) > 0$ is an appropriate constant that depends only on α_k, $0 < \tau < 3$ and our choices for the constants c_1 and c_2 in the last section, while $\varepsilon > 0$ is as yet unspecified.

Let us return to the empty fundamental parallelogram $\mathcal{P}_0 \in \Omega$ that avoids any splitting during the entire area magnification process of $\ell - c_2$ consecutive 3-cycles, resulting eventually in the parallelogram $\mathcal{P}_0^{(\ell-c_2)}$. Thus $\mathcal{P}_0^{(\ell-c_2)}$ is contained in a single X-face and has area

$$\alpha_k^{-3(\ell-c_2)} \cdot \frac{(4+o_k(1))\alpha_k^{3\ell}\alpha_k^{1/2}}{c_1^2} = \frac{(4+o_k(1))\alpha_k^{3c_2+1/2}}{c_1^2} = c_4,$$

where $c_4 = c_4(\alpha_k; \tau; c_1, c_2) > 0$ is an appropriate constant. Furthermore, in view of (4.17), the parallelogram $\mathcal{P}_0^{(\ell-c_2)}$ does not look like a long needle. Indeed, with constant size area c_4, the parallelogram $\mathcal{P}_0^{(\ell-c_2)}$ must contain a square of side length c_0 on some X-face, where $c_0 = c_0(\alpha_k; \tau; c_1, c_2) > 0$ is an appropriate small constant.

We are now ready to show that the Time-quantitative Density B contradicts the existence of the parallelogram $\mathcal{P}_0^{(\ell-c_2)}$.

Indeed, applying Time-quantitative Density B with $\kappa = c_0 = c_0(\alpha_k; \tau; c_1, c_2) > 0$, there exists a threshold $C^\star = C^\star(\kappa; \alpha_k) = C^\star(\alpha_k; \tau; c_1, c_2)$ such that if

$$\text{length}(\mathcal{L}_k(3(\ell - c_2))) \geqslant C^\star, \tag{6.4}$$

then $\mathcal{L}_k(3(\ell - c_2))$ intersects every square of side length c_0 on every X-face. In view of (6.3), it is clear that choosing

$$\varepsilon \leqslant \frac{c_3}{C^\star} \tag{6.5}$$

guarantees that (6.4) holds.

On the other hand, the parallelogram $\mathcal{P}_0^{(\ell-c_2)}$ is empty. Hence $\mathcal{L}_k(3(\ell - c_2))$ does not intersect $\mathcal{P}_0^{(\ell-c_2)}$, and so does not intersect any square of side length c_0 contained in $\mathcal{P}_0^{(\ell-c_2)}$.

This leads to a contradiction if we choose $\varepsilon > 0$ to satisfy (6.5) and also sufficiently small for the lower bound (4.24) to be valid. The choice of $\varepsilon > 0$ leads to suitable choices for n and m. Finally, the integer ℓ is determined by (6.2).

Thus we have established the following result.

Theorem 2. *Consider the concrete measure-preserving system $(X_0, \mathcal{A}, \lambda, T)$, where $X_0 = X_1 \cup X_2 \cup X_5$ is a polysquare surface related to the L-solid, $\mathcal{A}$ is the σ-algebra of Lebesgue-measurable subsets of X_0, λ is the 2-dimensional Lebesgue measure with $\lambda(X_0) = 3$, and $T = T_{\mathbf{v}_1} : X_0 \to X_0$ is a measure-preserving transformation defined via the $\mathbf{v}_1$-flow in the L-solid, and well defined for almost every point of X_0.*

Here $\mathbf{v}_1 = (1, \alpha_k, \alpha_k^2)$, where, for any arbitrary fixed integer $k \geqslant K_0$, where K_0 is an effectively computable absolute constant, α_k is a root of the cubic polynomial $x^3 + 2kx - 1$ satisfying (2.2).

Then the λ-measure-preserving transformation $T : X_0 \to X_0$ is ergodic.

We note that a set in the d-dimensional euclidean space $\mathbb{R}^d$ is said to be *Jordan measurable* if its 0-1-valued characteristic function has a well-defined d-dimensional Riemann integral.

From Theorem 2 we can deduce the following uniformity result.

Theorem 3. *Under the hypotheses of Theorem 2, for every Jordan measurable set $J \subset X_0$ and for almost every starting point $x \in X_0$, we have*

$$\lim_{m\to\infty} \frac{1}{m} \sum_{j=0}^{m-1} \chi_J(T^j x) = \frac{\lambda(J)}{3}, \tag{6.6}$$

where χ_J denotes the characteristic function of J and λ denotes the 2-dimensional Lebesgue measure.

Using the standard extension argument, this discrete result can be converted to the continuous version concerning the uniformity of geodesics in the L-solid with the special directions $\mathbf{v}_i$, $i = 0, 1, 2$, and almost every starting point. Here the test sets for uniformity are all 3-dimensional Jordan measurable subsets of the L-solid, and λ is replaced by the 3-dimensional Lebesgue measure.

Proof. Since $(X_0, \mathcal{A}, \lambda, T)$ is ergodic and λ is the 2-dimensional Lebesgue measure, it follows from Birkhoff's individual ergodic theorem that for almost every starting point $x \in X_0$, (6.6) holds in the special case when J is replaced by any Lebesgue-measurable set $A \subset X_0$.

Let $\mathcal{R} \subset \mathcal{A}$ denote the set of triangles in X_0 for which every vertex has rational coordinates. Since $\mathcal{R}$ is a countable set, and a countable union of zero-sets is a zero-set, it follows that for almost every starting point $x \in X_0$, (6.6) holds in the special case when J is replaced by any set $R \in \mathcal{R}$. Using the density of the rationals, it follows that for almost every starting point $x \in X_0$, (6.6) holds in the special case when J is replaced by any triangle $R \subset X_0$.

Every polygon is a finite union of triangles, so for almost every starting point $x \in X_0$, (6.6) holds in the special case when J is replaced by any polygon $P \subset X_0$.

The desired result now follows, since every Jordan measurable set can be well approximated by polygons. □

Note that Theorem 3 gives uniformity of geodesics for almost every starting point $x \in X_0$. We can extend the argument to give uniformity of geodesics for every *non-pathological* starting point $x \in X_0$. By a *non-pathological* starting point, we mean the starting point of a well-defined half-infinite geodesic in the L-solid, one that never hits a singular point where it becomes unclear how the orbit will continue. In other words, there is *no ambiguity as a consequence of hitting an edge.*

To illustrate this *orbit ambiguity*, consider the common edge of the faces X_4 and X_5 of the L-solid. As a consequence of the boundary identification of the L-solid, this edge is identified with the common edge of the faces X_1 and X_2, as shown in the picture on the left in Figure 6.1, and is also identified with the common edge of the faces Z_1 and Z_2, as shown in the picture on the right in Figure 6.1.

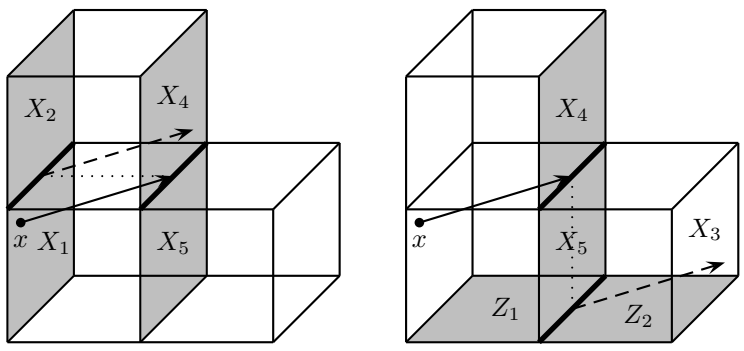

Figure 6.1: orbit ambiguity

Consider the starting point $x \in X_0$ shown in Figure 6.1, where $X_0 = X_1 \cup X_2 \cup X_5$. The transformation $T = T_{\mathbf{v}_1} : X_0 \to X_0$ maps x to a point Tx on the common edge of the faces X_4 and X_5. If we identify this edge with the common edge of the faces X_1 and X_2, then it is clear that T^2x lies on $X_4 = X_2$, as shown in the picture on the left in Figure 6.1. However, if we identify this edge with the common edge of the faces Z_1 and Z_2, then it is clear that T^2x lies on $X_3 = X_1$, as shown in the picture on the right in Figure 6.1.

Of course we do not want such a multi-valued map. The solution is very simple: we simply make a choice between the two options, and define T accordingly. Applying this simple recipe, it is easy to extend $T = T_{\mathbf{v}_1} : X_0 \to X_0$ on the *whole* compact flat surface X_0 such that T is *Jordan measurable*, *i.e.*, if $J \subset X_0$ is Jordan measurable, then $T^{-1}J \subset X_0$ is also Jordan measurable. Note that T is *not* continuous on X_0, but this is not a problem. Jordan measurability suffices for our purposes.

We shall establish the following generalization of Theorem 3 in the next section.

Theorem 4. *Under the hypotheses of Theorem 2, consider the measure-preserving Jordan measurable transformation $T = T_{\mathbf{v}_1} : X_0 \to X_0$, defined via the $\mathbf{v}_1$-flow in the L-solid and extended over the whole set X_0. Then for every Jordan measurable set $J \subset X_0$ and for every non-pathological starting point $x \in X_0$, we have*

$$\lim_{m\to\infty} \frac{1}{m} \sum_{j=0}^{m-1} \chi_J(T^j x) = \frac{\lambda(J)}{3},$$

where χ_J denotes the characteristic function of J and λ denotes the 2-dimensional Lebesgue measure.

Using the standard extension argument, this discrete result can be converted to the continuous version concerning the uniformity of geodesics in the L-solid with the special directions $\mathbf{v}_i$, $i = 0, 1, 2$, and every non-pathological starting point. Here the test sets for uniformity are all 3-dimensional Jordan measurable subsets of the L-solid, and λ is replaced by the 3-dimensional Lebesgue measure.

Since Birkhoff's ergodic theorem does not give any error term, both Theorems 3 and 4 are *time-qualitative* results concerning the uniformity of the orbits, and do not say anything about the speed of convergence to uniformity. However, we can essentially read out a time-quantitative result from the proof of Theorem 2. More precisely, we can slightly modify the proof, and derive a time-quantitative result concerning a weaker form of uniformity that we call *weak-uniformity*, which, roughly speaking, means uniformity apart from an absolute constant factor. Intuitively, this means that a *large nice* test set cannot be *grossly undervisited*.

Consider the discrete setting in Theorem 4. Let Q be a square on an X-face with side length $a > 0$, and let $T^j x_0$, $0 \leqslant j \leqslant m-1$, be a discrete orbit. Note that in the case of perfect uniformity, the expected number of members of this orbit that visit Q is equal to $a^2 m/3$. Suppose now that this orbit *grossly undervisits* Q, in the sense that there are less than $\varepsilon a^2 m/3$ members of this orbit that visit Q.

Repeating the arguments in Sections 4–6, we can then derive a contradiction if $\varepsilon > 0$ is sufficiently small, so that $\varepsilon \leqslant c(a; \alpha_k)$, where $c(a; \alpha_k) > 0$ is an effectively computable explicit positive constant that depends only on the side length a and the value of the direction parameter α_k.

On the X-face containing the given square Q, we consider the parallelogram lattice

$$\Omega = \Omega(\mathbf{u}_1, \mathbf{u}_2; \delta), \tag{6.7}$$

where any fundamental parallelogram $\mathcal{P} \in \Omega$ has sides $\delta \mathbf{u}_1$ and $\delta \mathbf{u}_2$. Here $\mathbf{u}_1$ and $\mathbf{u}_2$ are the critical eigenvectors defined in Section 4. The precise value of the parameter $\delta > 0$ will be specified later.

As before, we face the minor technical problem that the parallelogram lattice Ω in (6.7) does not tile the given square Q precisely. However, this has a negligible effect. With an appropriate choice of the parameters we can guarantee that there are more fundamental parallelograms $\mathcal{P} \in \Omega$ inside Q than those $\mathcal{P} \in \Omega$ that intersect the boundary of Q. Thus the total area of the fundamental parallelograms $\mathcal{P} \in \Omega$ with $\mathcal{P} \subset Q$ is greater than $a^2/2$.

The area of any fundamental parallelogram $\mathcal{P} \in \Omega$ is given by (4.14). We choose the parameter $\delta > 0$ so that

$$\text{area}(\mathcal{P}) = (4 + o_k(1))\delta^2 \alpha_k^{1/2} = \frac{3}{4\varepsilon m}.$$

By hypothesis, there are fewer than $\varepsilon a^2 m/3$ members of the discrete orbit $T^j x_0$, $0 \leqslant j \leqslant m-1$, that visit Q. Hence the total area of the fundamental parallelograms $\mathcal{P} \in \Omega$ that are visited by the orbit $T^j x_0$, $0 \leqslant j \leqslant m-1$, is less than

$$\frac{\varepsilon a^2 m}{3} \cdot \frac{3}{4\varepsilon m} = \frac{a^2}{4}. \tag{6.8}$$

Since the total area of all the fundamental parallelograms $\mathcal{P} \in \Omega$ with $\mathcal{P} \subset Q$ is greater than $a^2/2$, the bound (6.8) implies that the total area of the fundamental parallelograms $\mathcal{P} \in \Omega$ with $\mathcal{P} \subset Q$ not visited by the orbit $T^j x_0$, $0 \leqslant j \leqslant m-1$, is more than $a^2/4$. For simplicity, we refer to these $\mathcal{P} \subset Q$ as the *empty* fundamental parallelograms $\mathcal{P} \in \Omega$.

This lower bound $a^2/4$ on the number of empty fundamental parallelograms $\mathcal{P} \in \Omega$ is analogous to the lower bound (4.24). Thus we can repeat the entire argument in Sections 5 and 6, and arrive at the same contradiction just before Theorem 2, assuming that $\varepsilon \leqslant c(a; \alpha_k)$.

Thus we obtain the following time-quantitative *weak-uniformity* result.

Theorem 5. *Under the hypotheses of Theorem 2, consider the measure-preserving Jordan measurable transformation $T = T_{\mathbf{v}_1} : X_0 \to X_0$, defined via the $\mathbf{v}_1$-flow in the L-solid, where $\mathbf{v}_1$ is determined by the key parameter α_k with sufficiently large k, and extended over the whole set X_0. Let Q be a square on an X-face with side length $a > 0$, and let $T^j x_0$, $0 \leqslant j \leqslant m-1$, be a discrete orbit. Then there exist two effectively computable explicit positive constants $c_1 = c_1(a; \alpha_k) > 0$ and $c_2 = c_2(a; \alpha_k) > 0$, depending only on a and α_k, such that at least $c_1 m$ members of this orbit visit Q, provided that $m \geqslant c_2$.*

Using the standard extension argument, this discrete result can be converted to the continuous version concerning the weak-uniformity of geodesics in the L-solid with the special directions $\mathbf{v}_i$, $i = 0, 1, 2$. More precisely, let Q be a cube inside the L-solid with side length $a > 0$, and let $L(t)$, $0 \leqslant t \leqslant T$, be a finite geodesic segment with any of the special directions $\mathbf{v}_i$, $i = 0, 1, 2$, with arc-length parametrization. Then there exist two effectively computable explicit positive constants $c_3 = c_3(a; \alpha_k) > 0$ and $c_4 = c_4(a; \alpha_k) > 0$ such that a particle moving with unit speed on the given geodesic segment spends time at least equal to $c_3 T$ inside the cube Q, provided that $T \geqslant c_4$.

Since every 3-dimensional Jordan measurable set A can be well approximated by a disjoint union of a finite number of cubes, we have the following more general result. There exist two effectively computable explicit positive constants $c_5 = c_5(A; \alpha_k) > 0$ and $c_6 = c_6(A; \alpha_k) > 0$ such that a particle moving with unit speed on the given

special geodesic segment spends time at least equal to c_5T inside the set A, provided that $T \geqslant c_6$.

The proofs of Theorems 2–5 given for the L-solid have rather straightforward extensions to any polycube 3-manifold with 1-direction geodesic flow. We include the details at the end of the next section.

7. Unique ergodicity: proving Theorems 4 and 1

Unique ergodicity refers to the extension of Theorems 2 and 3 where we replace uniformity for almost every starting point to uniformity for every non-pathological starting point. The pioneering results on *unique ergodicity* are due to Furstenberg [3, Sections 3.2–3.3]. The reader, however, does not need to know those sections. For the sake of completeness, we have included here the necessary arguments.

Proof of Theorem 4. The proof goes by contradiction, and consists of two parts. In the first part, we simply follow Furstenberg's argument. The surprising basic idea here is a reformulation of the problem in terms of T-invariant Borel measures and the use of functional analysis. The second part is an *ad hoc* argument based on some special simultaneous diophantine approximation properties of the given direction vectors $\mathbf{v}_i$, $i = 0, 1, 2$, associated to real algebraic numbers of degree 3.

The first part of the argument is summarized in the following lemma.

Lemma 7.1. *Suppose that there exist a non-pathological starting point $y_0 \in X_0$ and a Jordan measurable set $J_0 \subset X_0$ for which uniformity fails, so that the infinite sequence*

$$\frac{1}{m}\sum_{j=0}^{m-1} \chi_{J_0}(T^j y_0), \quad m \geqslant 1, \tag{7.1}$$

where χ_{J_0} is the characteristic function of J_0, does not converge to $\lambda(J_0)/3$. Then there exists an ergodic measure-preserving system $(X_0, \mathcal{B}, \nu, T)$, where $\mathcal{B}$ is the Borel σ-algebra on X_0 and ν is a new T-invariant Borel probability measure, such that

$$\nu(J_0) \neq \frac{\lambda(J_0)}{\lambda(X_0)} = \frac{\lambda(J_0)}{3}. \tag{7.2}$$

Proof. In view of the assumption, there exists an infinite subsequence

$$0 \leqslant h_0 < h_1 < h_2 < h_3 < \ldots$$

of the positive integers such that the limit

$$\lim_{m\to\infty} \frac{1}{h_m}\sum_{j=0}^{h_m-1} \chi_{J_0}(T^j y_0),$$

exists, but is not equal to $\lambda(J_0)/3$.

We now repeat and adapt some ideas in [3, Sections 3.2–3.3]. For every integer $m \geqslant 1$, we introduce the normalized counting measure ν_m, defined for every Borel set $B \subset X_0$ by

$$\nu_m(B) = \frac{1}{h_m}\sum_{j=0}^{h_m-1} \chi_B(T^j y_0), \tag{7.3}$$

where χ_B is the characteristic function of B.

Now we make use of a general theorem in functional analysis which says that the space of Borel probability measures on any compact set is compact in the so-called *weak-star topology*. The latter means that

$$\mu_m \to \mu \quad \text{if and only if} \quad \int f \,\mathrm{d}\mu_m \to \int f \,\mathrm{d}\mu,$$

where f runs over all continuous functions on the compact space.

This compactness theorem is a non-trivial result. The standard proof is based on the Riesz Representation Theorem.

Let $\mathcal{M}$ denote the set of Borel probability measures μ on X_0. By the general theorem, $\mathcal{M}$ is compact. Let $\mathcal{M}_1 \subset \mathcal{M}$ denote the set of those Borel probability measures μ on X_0 that are T-invariant and such that $\mu \neq \lambda/3$. It is obvious that $\mathcal{M}_1$ is a closed subset of $\mathcal{M}$ and therefore compact.

The compactness of $\mathcal{M}$ implies that there is a subsequence ν_{m_i} of the sequence ν_m defined by (7.3) such that $\nu_{m_i} \to \nu_\infty$ as $i \to \infty$, where ν_∞ is a Borel probability measure on X_0. It easily follows from (7.3) that ν_∞ is T-invariant. Indeed, writing $y_1 = Ty_0$, we have

$$\begin{aligned}
\nu_m(T^{-1}B) &= \frac{1}{h_m} \sum_{j=0}^{h_m-1} \chi_B(T^j y_1) = \frac{1}{h_m} \sum_{j=1}^{h_m} \chi_B(T^j y_0) \\
&= \frac{1}{h_m} \sum_{j=0}^{h_m-1} \chi_B(T^j y_0) + \frac{\chi_B(T^{h_m} y_0) - \chi_B(y_0)}{h_m} \\
&= \nu_m(B) + \frac{\chi_B(T^{h_m} y_0) - \chi_B(y_0)}{h_m},
\end{aligned}$$

and

$$\left| \frac{\chi_B(T^{h_m} y_0) - \chi_B(y_0)}{h_m} \right| \leqslant \frac{1}{h_m} \to 0 \quad \text{as } m \to \infty.$$

Moreover, the limit measure ν_∞ clearly satisfies the requirement in (7.2), implying that $\nu_\infty \in \mathcal{M}_1$, and so $\mathcal{M}_1$ is a non-empty compact set.

To find an appropriate $\nu \in \mathcal{M}_1$ which guarantees that the measure-preserving system $(X_0, \mathcal{B}, \nu, T)$ is ergodic, we use the almost trivial fact that $\mathcal{M}_1$ is convex. The well known Krein–Milman theorem in functional analysis implies that the non-empty convex set $\mathcal{M}_1$ is spanned by its *extremal points*. It is a well known general result in ergodic theory that the extremal points are precisely the ergodic T-invariant measures; see [3, Proposition 3.4]. Thus we can choose our measure $\nu \in \mathcal{M}_1$ to be such an extremal point, and this completes the proof. □

The remainder of the proof is concerned with showing that the conclusion of Lemma 7.1 leads to a contradiction by using some very special number-theoretic properties of the cubic algebraic number α_k which defines the direction vector.

Since the measure-preserving system $(X_0, \mathcal{B}, \nu, T)$ given by Lemma 7.1 is ergodic, it follows from Birkhoff's ergodic theorem that for every Borel set $B \in \mathcal{B}$ and for ν-almost every $y \in X_0$, we have

$$\lim_{m\to\infty} \frac{1}{m} \sum_{j=0}^{m-1} \chi_B(T^j y) = \nu(B). \tag{7.4}$$

Let W be an arbitrarily large but fixed positive integer. We claim that there exists a non-empty open square $Q = Q(W) \subset X_0$ such that

$$\frac{\nu(Q)}{\lambda(Q)} > W. \tag{7.5}$$

To prove (7.5), we choose $B = J_0$ in (7.1), and consider the set

$$Y = \left\{ y \in X_0 : \lim_{m\to\infty} \frac{1}{m} \sum_{j=0}^{m-1} \chi_{J_0}(T^j y) = \nu(J_0) \right\}. \tag{7.6}$$

We already know from Theorem 3 that for λ-almost every $y \in X_0$, we have

$$\lim_{m\to\infty} \frac{1}{m} \sum_{j=0}^{m-1} \chi_{J_0}(T^j y) = \frac{\lambda(J_0)}{3}, \tag{7.7}$$

where λ denotes the 2-dimensional Lebesgue measure. Combining (7.2), (7.4), (7.6) and (7.7), we conclude that

$$\nu(Y) = 1 \quad \text{and} \quad \lambda(Y) = 0. \tag{7.8}$$

Let $\delta > 0$ be arbitrarily small but fixed. Since $\lambda(Y) = 0$, there exists an infinite sequence R_i, $i \geqslant 1$, of open squares such that

$$\sum_{i=1}^{\infty} \lambda(R_i) < \delta \quad \text{and} \quad Y \subset \bigcup_{i=1}^{\infty} R_i. \tag{7.9}$$

By (7.8) and (7.9), we have

$$\sum_{i=1}^{\infty} \nu(R_i) \geqslant 1. \tag{7.10}$$

It follows from (7.9) and (7.10) that there exists an integer $i_0 \geqslant 1$ such that

$$\frac{\lambda(R_{i_0})}{\nu(R_{i_0})} < \delta. \tag{7.11}$$

Choosing $\delta = 1/W$ in (7.11), the inequality (7.5) follows with the choice $Q = R_{i_0}$.

We next take advantage of the special direction vector $\mathbf{v}_1 = (1, \alpha_k, \alpha_k^2)$, where α_k is a cubic algebraic number given by (2.1) and (2.2). We apply some general results from diophantine approximation, summarized in the next two lemmas. We use the standard notation $\|x\|$ to denote the distance of a real number x from the nearest integer.

The first lemma concerns badly approximable linear forms; see [10, Chapter II, Theorem 4A].

Lemma 7.2. *Let $m \geqslant 1$ be an integer, and let $\gamma_1, \ldots, \gamma_m$ be any m numbers in a real algebraic number field of degree $m+1$ such that $1, \gamma_1, \ldots, \gamma_m$ are linearly independent over the rationals. Write $\mathbf{v} = (1, \gamma_1, \ldots, \gamma_m) \in \mathbb{R}^{m+1}$. Then there exists a constant $C > 0$, depending at most on m and $\gamma_1, \ldots, \gamma_m$, such that*

$$\left\| \sum_{i=1}^{m} n_i \gamma_i \right\| \geqslant \frac{C}{(\max_{1\leqslant i\leqslant m} |n_i|)^m} \tag{7.12}$$

for every $\mathbf{n} = (n_1, \ldots, n_m) \in \mathbb{Z}^m$ with $\mathbf{n} \neq \mathbf{0}$.

We comment that (7.12) follows relatively easily from the definition of the *norm* in an algebraic number field.

The second lemma is Mahler's transference theorem in the relevant special case; see [7] or [2, Chapter 5, Theorem 2].

Lemma 7.3. *A necessary and sufficient condition that there exists a constant $C_1 > 0$ such that*

$$\left\| \sum_{i=1}^{m} n_i \gamma_i \right\| \left(\max_{1 \leqslant i \leqslant m} |n_i| \right)^m \geqslant C_1$$

for every $\mathbf{n} = (n_1, \ldots, n_m) \in \mathbb{Z}^m$ with $\mathbf{n} \neq \mathbf{0}$, is that there exists another constant $C_2 > 0$ such that

$$\left(\max_{1 \leqslant j \leqslant m} \|n\gamma_j\| \right)^m |n| \geqslant C_2$$

for every $n \in \mathbb{Z}$ with $n \neq 0$.

Let $\gamma_1 = \alpha_k$ and $\gamma_2 = \alpha_k^2$. It follows from Lemma 7.2 that there exists a constant $C = C(\alpha_k) > 0$, depending only on α_k, such that

$$\|n_1\alpha_k + n_2\alpha_k^2\| \geqslant \frac{C}{(\max\{|n_1|, |n_2|\})^2}$$

for every $\mathbf{n} = (n_1, n_2) \in \mathbb{Z}^2$ with $\mathbf{n} \neq \mathbf{0}$. It then follows from Lemma 7.3 that there exists another constant $C' = C'(\alpha_k) > 0$, depending only on α_k, such that

$$(\max\{\|n\alpha_k\|, \|n\alpha_k^2\|\})^2 |n| \geqslant C' \tag{7.13}$$

for every $n \in \mathbb{Z}$ with $n \neq 0$.

Consider the 2-dimensional vector $\mathbf{w}_1 = (\alpha_k, \alpha_k^2)$. Note that the transformation $T = T_{\mathbf{v}_1} : X_0 \to X_0$ *modulo one* reduces to the $\mathbf{w}_1$-shift

$$\mathbf{x} \to \mathbf{x} + \mathbf{w}_1 \bmod [0,1)^2 \tag{7.14}$$

on the flat unit torus $[0,1)^2$.

Applying (7.4) in the case when B is the non-empty open square $Q = Q(W)$, we deduce that for ν-almost every $z \in X_0$, we have

$$\lim_{m \to \infty} \frac{1}{m} \sum_{j=0}^{m-1} \chi_Q(T^j z) = \nu(Q), \tag{7.15}$$

where χ_Q is the characteristic function of Q. Let $z = z_0$ in X_0 satisfy (7.15). Then there exists a threshold m_0 such that for every $m \geqslant m_0$, we have

$$\frac{1}{m} \sum_{j=0}^{m-1} \chi_Q(T^j z_0) = \frac{\nu(Q)}{2}. \tag{7.16}$$

Choosing m sufficiently large, we can guarantee that $1/\sqrt{m}$ is *much* smaller than the side length of the square Q. We divide Q into small congruent subsquares R_i, $i \in I$, of side length $1/r$, where $m = C'r^2$ and $C' > 0$ is the constant in (7.13). Thus if we ignore, for notational simplicity, those small squares R_i that intersect the boundary of Q, then with negligible error if m is sufficiently large, we have

$$Q = \bigcup_{i \in I} R_i, \quad |I| = \lambda(Q) r^2. \tag{7.17}$$

We claim that

$$T^{-j_1} R_i \cap T^{-j_2} R_i = \emptyset, \quad i \in I,\ 0 \leqslant j_1 < j_2 \leqslant m-1. \tag{7.18}$$

Suppose, on the contrary, that there exist $i \in I$ and integers $0 \leqslant j_1 < j_2 \leqslant m-1$ such that $T^{-j_1}R_i$ intersects $T^{-j_2}R_i$. Let

$$\mathbf{u} \in T^{-j_1}R_i \cap T^{-j_2}R_i.$$

Then both $T^{j_1}\mathbf{u}$ and $T^{j_2}\mathbf{u}$ are elements of the same small square R_i of side length $1/r$. Applying the *modulo one* reduction in (7.14), we see that $\mathbf{u} + j_1\mathbf{w}_1$ and $\mathbf{u} + j_2\mathbf{w}_1$ are $1/r$-close to each other on the flat torus $[0,1)^2$, and so $(j_2 - j_1)\mathbf{w}_1$ and $\mathbf{0} = (0,0)$ are $1/r$-close to each other on the flat torus $[0,1)^2$. Thus

$$(\max\{\|(j_2 - j_1)\alpha_k\|, \|(j_2 - j_1)\alpha_k^2\|\})^2 \leqslant \frac{1}{r^2} = \frac{C'}{m}. \tag{7.19}$$

On the other hand, applying (7.13) with $n = j_2 - j_1$, we obtain

$$(\max\{\|(j_2 - j_1)\alpha_k\|, \|(j_2 - j_1)\alpha_k^2\|\})^2 \geqslant \frac{C'}{j_2 - j_1} > \frac{C'}{m},$$

contradicting (7.19). This establishes (7.18).

We are ready to complete the proof of Theorem 4. Combining (7.16) and (7.17), we have, for every $m \geqslant m_0$,

$$\frac{\nu(Q)m}{2} \leqslant \sum_{j=0}^{m-1} \chi_Q(T^j z_0) = \sum_{i \in I} \sum_{j=0}^{m-1} \chi_{R_i}(T^j z_0) \leqslant |I|, \tag{7.20}$$

where the last inequality is a consequence of (7.18).

Combining (7.5), (7.17), (7.19) and (7.20), we conclude that

$$W < \frac{\nu(Q)}{\lambda(Q)} \leqslant \frac{2}{C'}.$$

But this is absurd, since $2/C'$ is a constant depending only on α_k, and W can be arbitrarily large. This completes the proof of Theorem 4. □

Finally, we discuss how we can extend Theorems 2–5 concerning the L-solid to any polycube 3-manifold with 1-direction geodesic flow, and establish Theorem 1.

Let $\mathcal{P}$ be an arbitrary polycube 3-manifold. Our task is to extend the proof of Theorem 2 given in the special case of the L-solid with street-LCM equal to 2 to the case of $\mathcal{P}$ with 1-direction geodesic flow. We know that $\mathcal{P}$ has X-streets, Y-streets, and Z-streets, and that the street-LCM of $\mathcal{P}$ is the least common multiple of the lengths of all the streets.

We can clearly adapt Sections 3–5, as the discussion in these sections does not use any special property of the L-solid that is not present in an arbitrary polycube 3-manifold. For notational convenience, and for easy visualization, we have chosen to work earlier with the simplest concrete special case of the L-solid.

In order to generalize the argument in Section 6, we need a time-quantitative density result for any polycube 3-manifold. The following result is [1, Theorem 6.4.2], and is a straightforward generalization of Time-quantitative Density A in Section 2.

Let $\eta > 0$ be an arbitrarily small but fixed positive number. We say that a half-infinite geodesic $\mathcal{L}$ in $\mathcal{P}$ is *η-nearly superdense* if there exists an effectively computable explicit threshold $N_0(\mathcal{P};\eta)$ such that, for every integer $n \geqslant N_0(\mathcal{P};\eta)$, the initial segment of $\mathcal{L}$ with length $n^{2+\eta}$ intersects every axis-parallel cube of side length $1/n$ in $\mathcal{P}$.

Lemma 7.4. *Let $\mathcal{P}$ be an arbitrary polycube 3-manifold, and let $h = h(\mathcal{P})$ denote the street-LCM of $\mathcal{P}$. Let $\eta > 0$ be fixed. There exists a threshold $K_0(\mathcal{P};\eta)$ such that for every integer $k \geqslant K_0(\mathcal{P};\eta)$, any half-infinite geodesic in $\mathcal{P}$ with direction given by*

one of the vectors in (1.2)*, where* α_k *is a root of the cubic equation* $x^3 + hkx - 1 = 0$ *in the interval*

$$\frac{1}{hk+1} < \alpha_k < \frac{1}{hk},$$

is η*-nearly superdense in* $\mathcal{P}$*.*

Using this density result, it is fairly straightforward to generalize the argument in Section 6 to establish an analog of Theorem 2 for any polycube 3-manifold. Finally, repeating the arguments in the derivation of Theorems 3–5 from Theorem 2, we can complete the proof of Theorem 1.

References

[1] J. Beck, W.W.L. Chen, Y. Yang. Quantitative behavior of non-integrable systems (III). `arxiv.org/abs/2006.06213`, 93 pp.

[2] J.W.S. Cassels. *An Introduction to Diophantine Approximation* (Cambridge University Press, 1957).

[3] H. Furstenberg. *Recurrence in Ergodic Theory and Combinatorial Number Theory* (Princeton University Press, 1981).

[4] E. Gutkin. Billiards on almost integrable polyhedral surfaces. *Ergodic Theory Dynam. Systems* **4** (1984), 569–584.

[5] P. Hubert, T.A. Schmidt. An introduction to Veech surfaces. *Handbook of Dynamical Systems* (B. Hasselblatt, A. Katok, eds.), volume 1B, pp. 501–526 (Elsevier, 2006).

[6] D. König, A. Szücs. Mouvement d'un point abondonne a l'interieur d'un cube. *Rend. Circ. Mat. Palermo* **36** (1913), 79–90.

[7] K. Mahler. Ein Übertragungsprinzip für lineare Ungleichungen. *Časopis Pěst. Math. Fys.* **68** (1939), 85–92.

[8] H. Masur. Ergodic theory of translation surfaces. *Handbook of Dynamical systems* (B. Hasselblat, A. Katok, eds.), vol. 1B, pp. 527–547 (Elsevier, 2006).

[9] H. Masur, S. Tabachnikov. Rational billiards and flat surfaces. *Handbook of Dynamical systems* (B. Hasselblat, A. Katok, eds.), vol. 1A, pp. 1015–1089 (Elsevier, 2006).

[10] W.M. Schmidt. *Diophantine Approximation* (Lecture Notes in Mathematics **785**, Springer, 1980).

[11] W.A. Veech. Boshernitzan's criterion for unique ergodicity of an interval exchange transformation. *Ergodic Theory Dynam. Systems* **7** (1987), 149–153.

[12] H. Weyl. Über die Gleichverteilung von Zahlen mod. Eins. *Math. Ann.* **77** (1916), 313–352.

[13] A. Zorich. Flat surfaces. *Frontiers in Number Theory, Physics, and Geometry* (P.E. Cartier, B. Julia, P. Moussa, P. Vanhove, eds.), vol. 1, pp. 439–586 (Springer, 2006).

Department of Mathematics, Rutgers University, Hill Center for the Mathematical Sciences, Piscataway NJ 08854, USA

Email address: `jbeck@math.rutgers.edu`

Department of Mathematics and Statistics, Macquarie University, Sydney NSW 2109, Australia

Email address: `william.chen@mq.edu.au`